Available online at www.sciencedirect.com
ScienceDirect
Journal of Computational Physics 225 (2007) 1937–1960
JOURNAL OF COMPUTATIONAL PHYSICS
www.elsevier.com/locate/jcp

A volume of fluid method for a two-dimensional plasma expansion problem

K.-C. Le Thanh [a], C. Parzani [b], M.-H. Vignal [b,*]

[a] *CEA/DAM Ile de France, 92500 Bruyéres le Châtel Cedex, France*
[b] *MIP, Institut de Mathématiques de Toulouse UMR 5219 (CNRS-UPS-INSA-UT1), Université Toulouse 3, 31062 Toulouse Cedex 9, France*

Received 20 July 2006; received in revised form 21 February 2007; accepted 23 February 2007
Available online 14 March 2007

Abstract

This paper is devoted to the numerical study of a two-dimensional model for plasma expansion in vacuum. The plasma, constituted of ions and electrons, is injected from a part of the cathode and undergoes a thermal expansion. Due to the positive anode potential, electrons are emitted from the plasma–vacuum interface, forming an electron beam. Moreover, electron emission produces a reaction-pressure force which slows down the plasma expansion. Previous works [P. Degond, C. Parzani, M.H. Vignal, Un modéle d'expansion de plasma dans le vide, C. R. Acad. Sci. Paris 335 (2002) 399; P. Degond, C. Parzani, M.H. Vignal, Plasma expansion in vacuum: modeling the breakdown of quasineutrality, SIAM, Multiscale Model. Simul. 2 (2003) 158; P. Degond, C. Parzani, M. H. Vignal, A model for plasma expansion in the vacuum, in: Proceedings of the Conference ''Free Boundary Problems 2002'', Trento, June 2002] have been realized to describe this process in the one-dimensional case. One of the main goal is to get a precise description of the interface motion. The aim of the present work is to explore more realistic cases investigating a two-dimensional model. However, considering upper dimensions yields to new difficulties essentially from a numerical point of view. Indeed, in the 2D space case, the plasma–vacuum interface is no more a point but a curve. Therefore, in this work, after proposing a two-dimensional model, we focus on the interface tracking using a volume of fluid method. We perform numerical simulations on two test cases. The first test case consists in a two-dimensional fluid compression for which an analytic solution is known. The second test case is the plasma bubble expansion between two electrodes.

Keywords: Plasma expansion; Quasi-neutral limit; Child–Langmuir law; Volume of fluid method; Plasma–vacuum interface

1. Introduction

In this article, we are interested in the two-dimensional numerical modeling of a plasma expanding in the vacuum between two electrodes. This plasma is assumed quasi-neutral and constituted of one ion species and

* Corresponding author. Tel.: +33 5 61 55 69 22; fax: +33 5 61 55 83 85.
E-mail addresses: kim-claire.le-thanh@cea.fr (K.-C. Le Thanh), parzani@mip.ups-tlse.fr (C. Parzani), mhvignal@mip.ups-tlse.fr (M.-H. Vignal).

0021-9991/$ - see front matter © 2007 Elsevier Inc. All rights reserved.
doi:10.1016/j.jcp.2007.02.031

of electrons. It is injected from a part of the cathode and undergoes a thermal expansion in the gap between the electrodes. During its expansion, attracted by the high positive potential of the anode, some electrons are emitted in the gap. They form a beam in the vacuum. Then, the device is divided in two regions with different characteristic properties: the plasma region which is a quasi-neutral zone and the beam region where there are only electrons.

We use a fluid description, then all the device, between the cathode and the anode, can be described using a two-fluid model constituted of the Euler equations for each species coupled with the Poisson equation for the potential. Unfortunately this model has some severe numerical constraints (see [19]). They are related to the so-called Debye length and electron plasma period, well known in plasma physics (see [5,29]). The Debye length is the typical length at which electric interactions occur and the electron plasma period is the period of the electrons oscillations around their equilibrium position. They are both inversely proportional to the square root of the quasi-neutral plasma density. In a numerical point of view, in classical discretizations, the space and time steps must resolve these scales in order to prevent instabilities.

Here, we are interested in two physical applications, the first application deals with high current plasma diodes, see [30,34,48,55,58]. In this case, the plasma is used to increase the extracted current as compared with conventional plane diodes. The second application concerns electrical discharges on satellite solar panels and more precisely the transition from the primary discharge to the electric arc, see [6,18,24,28]. Note that this study can be also applied to electron beam driven flash X-ray radiography problems, see [33] for a detailed review of recent advances. Furthermore, the physical problems studied here have strong analogies with the ion sheath problem see [23,41,50,51] and references therein. Then, in the physical applications we are interested in (high current plasma diodes and electrical discharges on satellite solar panels), the densities in the plasma are very high. Therefore, the associated Debye length and plasma period are very small. This yields to numerical simulations in two dimensions, too much expensive to be done in practice.

There are two possible ways to overcome this limitation. The first way, chosen in [11,7,9,45,49], consists in finding an asymptotically stable discretization, i.e. a scheme which does not require the resolution of the small scales of the plasma period and of the Debye length. The second way, chosen in [10,12,13] for one-dimensional problems and that we choose here, consists in finding an asymptotic model in the quasi-neutral region, the discretizations of such a model do no require to resolve the plasma period and the Debye length. In [10,12,13], different one-dimensional models are proposed. They consist in quasi-neutral models for the plasma region and a Child–Langmuir model for the beam region. They are all obtain letting formally tend the Debye length to zero in the initial two fluid model with different assumptions for each models.

In [12] the plasma is assumed to be a free current plasma. The resulting asymptotic quasi-neutral model, for the description of the plasma, is the Euler system for the quasi-neutral density $n = n_i = n_e$ and the total momentum $q = (m_i + m_e)n\mathbf{u}$ where n_i, n_e and $\mathbf{u}_i = \mathbf{u}_e = \mathbf{u}$ are the ion and electron densities and velocities, furthermore m_i and m_e are the particle masses. For the description of the beam, we derived a Child–Langmuir model (see [31]) which has an explicit solution in one dimension (see [16]). The key point of the modelization is the connection between the two regions. Basing on one-dimensional simulations of the two-fluid model, we assume that the beam exerts a force on the plasma. This force, called in the following the ''pressure reaction force'', slows down the plasma expansion and creates a shock at the plasma–beam interface. Then using Rankine–Hugoniot relations we determine the pressure reaction and the velocity of the interface, note that the velocity is given by the ion velocity at the plasma–beam interface. The one-dimensional numerical simulations of this model (see [12] for the isentropic case and [14] for full Euler equations) show that this model leads to the right interface velocity. But it gives an overflow in the density results near the interface. This is due to the fact that the ''pressure reaction force'' is concentrated at the interface.

In order to overcome this problem, we proposed in [13] a one-dimensional quasi-neutral model with a non-vanishing current for the description of the plasma. One of the formulations of this model is constituted of the isentropic Euler equations for the quasi-neutral density and the total momentum but with some additional terms in the flux of the conservation momentum equation. These additional terms depend on the current which is constant in all the device and is given by the Child–Langmuir current of the beam region. These terms express the reaction of the beam region onto the plasma region. Note that in this case the pressure reaction force is exerted in all the plasma and not only at the interface. The numerical simulations of this model show

a very good agreement with the results of the two-fluid model simulations. Unfortunately this formulation is ill posed in two dimensions. In [10], we proposed and compared different formulations of this model which can be used in two dimensions. These formulations are all given by hyperbolic systems with an implicit nonlinear constraint. This constraint makes these formulations difficult to solve numerically.

Now, the aim of this article is to explore more realistic situations studying the two-dimensional space case. The interface is then a curve which leads to new difficulties in the modeling as well as in the numerical scheme. Here, we want to focus our attention on the difficulties related to the numerical simulation of the plasma–beam interface. For these reasons we use the zero current model presented in [12] which is simpler to discretize.

We begin this article with the description of the two-dimensional mathematical model in Section 2. Following the idea of [12], by a formal asymptotic analysis, from the two-fluid Euler Poisson model, we derive a quasi-neutral model for the plasma zone. This model is constituted of the isentropic Euler equations for the quasi-neutral fluid. For the beam region we choose a simplified model. It consists in assuming that the one-dimensional Child–Langmuir law can be applied. For all points of the plasma–beam interface, knowing the distance covered by an electron from this point to the anode, the one-dimensional Child–Langmuir law gives the current at the plasma–beam interface point. We propose a simple method to approximate this covered distance.

In Section 3, we present the numerical scheme. Note that the main difficulty is the plasma–beam interface discretization. We consider this problem as a problem of an interface separating two fluids: the plasma and the vacuum of plasma. There are several families of methods used in the literature for the numerical simulations of moving interfaces. A detailed review of these families is done in [43,52]. The first family, see [1,25,35] and references therein, consists in Lagrangian methods in which the mesh follows the fluid. When there are large fluid displacements, the mesh can suffer of large distortions and it is necessary to rezoning periodically. Then, there is the interface tracking family. It consists in discretizing the interface with some points and in following their positions on an Eulerian mesh, for further details, one can see [21,22,56,40]. Finally, there are the Eulerian methods family with the ''volume of fluid'' and level set methods. The main idea of the volume of fluid methods (see [26]) consists in following the interface with the volume fraction of the fluid in all the cells of the mesh. This volume fraction is updated at each time step determining the advected quantity of fluid from a cell to its neighbors (see [59]). One can see [3,8,42,44] for recent developments. In the level set methods the interface is defined as a zero level set of a continuous function advected with the fluids velocity. This method was introduced in [38] and has been further developed in [4,27,53,54], one can also see the books [37,47].

We chose to use a VOF method because we wanted an Eulerian method in order to use a simple fixed Cartesian mesh and because it seems to us well adapted to take into account of the pressure reaction force at the plasma–beam interface. For all cells of the mesh and all time step the unknowns are the volume fraction of each fluids present in the cell and the averaged fluid variables (densities, velocities, etc.). These averaged quantities are advected using a Lagrangian scheme. Then a projection step gives the advected volume fraction and averaged fluid variables on the Eulerian mesh. Here we use the SLIC algorithm (for simple line interface calculation, see [36]) to define the transfer priorities of the plasma in the cells of the mesh. In our applications, the main difficulty consists in taking into account at the discrete level of the ''pressure reaction'' term acting along the interface. To this aim, we need to localize the plasma–beam interface. Then, we use Young's method (see [60]) which gives an oblique representation of the interface.

In Section 4, we present numerical results. We begin with a test case of a two-dimensional fluid compression. The fluid is initially located in a ball and a uniform pressure applied on its boundary compresses it toward the radius center. Since we know an analytic solution we can study the accuracy of our discretization. We conclude this article with numerical simulations for high current diodes, we simulate the plasma bubble expansion between two electrodes.

2. Presentation of the model

Here, we present the two-dimensional model used for the description of the plasma bubble expansion in the gap between two electrodes. We recall that it is a two-dimensional model which is an extension of the one-dimensional zero current model given in [12]. We begin with the presentation of the different regions and their

dynamics. Then we give the quasi-neutral model for the plasma region and the simplified Child–Langmuir model valid in the beam region.

2.1. The different regions and their dynamic

We consider the device shown in Fig. 1. The cathode Γ_K is defined by $\Gamma_K = \{(x,y) \in \mathbb{R}^2;\ x = f_K(y) \text{ and } y \in [a,b]\}$ and the anode by $\Gamma_A = \{(x,y) \in \mathbb{R}^2;\ x = f_A(y) \text{ and } y \in [a,b]\}$ where a and b are given reals and $f_K : [a,b] \to \mathbb{R}$ and $f_A : [a,b] \to \mathbb{R}$ are given smooth functions. We define the artificial boundary by $\Gamma_{art} = [f_K(a), f_A(a)] \times \{a\} \cup [f_K(b), f_A(b)] \times \{b\}$. Then, we consider the domain Ω delimited by Γ_K, Γ_A and Γ_{art} as shown in Fig. 1. The particles are injected from a part of the cathode and the plasma bubble, Ω_P, expands in the domain Ω. Note that the domain Ω is chosen sufficiently large such that the artificial boundary Γ_{art} is far from the plasma region during all the simulation.

We describe the particles in the domain Ω by their density and their velocity n_i, $\mathbf{u}_i$ for the ions and n_e, $\mathbf{u}_e$ for the electrons. Furthermore, we denote by ϕ the electric potential and we suppose that $\phi_{|\Gamma_K} = 0$. Following [12], we assume that the plasma region, i.e. the region filled by the quasi-neutral plasma, is given, for all $t > 0$, by

$$\Omega_P(t) = \{(x,y) \in \Omega, y \in \mathbb{R} \text{ and } x < \sup\{\xi \in \mathbb{R}; n_i(\xi', y, t) > 0\ \forall \xi' \in [0,\xi]\}\}. \tag{1}$$

Then the plasma–beam interface and the beam region are, respectively, defined by

$$\Gamma(t) = \partial\Omega_P(t) \cap \Omega \quad \text{and} \quad \Omega_B(t) = \Omega \setminus (\Omega_P \cup \Gamma(t)). \tag{2}$$

The plasma region is characterized by the presence of ions, then it moves with the ions velocity, i.e. for all $X = (x,y) \in \Gamma(t)$ we have

$$\frac{dX}{dt} = \mathbf{u}_i(X,t). \tag{3}$$

The two-dimensional model consists in using the quasi-neutral model, given in Section 2.2, for the plasma region Ω_P and the simplified Child–Langmuir model, given in Section 2.3 for the beam region Ω_B.

2.2. The quasi-neutral model in the plasma region

For describing the plasma, we use a two-dimensional quasi-neutral model with a vanishing current. It is given by the Euler equations for the density n and the total momentum $n\mathbf{u}$ of the plasma. We write for all $t > 0$ and all $(x,y) \in \Omega_P(t)$:

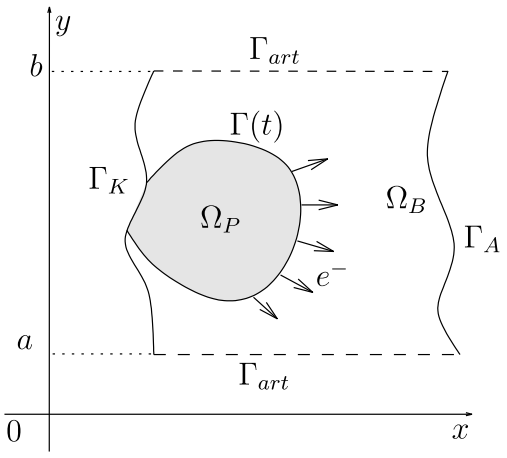

Fig. 1. The two-dimensional device: the plasma bubble, Ω_P, expands between the cathode Γ_K and the anode Γ_A, during its expansion some electrons are emitted in the vacuum forming a beam in Ω_B.

$$\begin{aligned}
&\phi(x,y,t) = 0,\\
&n_{\mathrm{i}}(x,y,t) = n_{\mathrm{e}}(x,y,t) = n(x,y,t), \quad \mathbf{u}_{\mathrm{i}}(x,y,t) = \mathbf{u}_{\mathrm{e}}(x,y,t) = \mathbf{u}(x,y,t),\\
&\partial_t n(x,y,t) + \nabla\cdot(n(x,y,t)\mathbf{u}(x,y,t)) = 0,\\
&(m_{\mathrm{i}}+m_{\mathrm{e}})(\partial_t(n\mathbf{u})(x,y,t) + \nabla\cdot(n\mathbf{u}\otimes\mathbf{u})(x,y,t)) + \nabla p(n(x,y,t)) = 0,
\end{aligned} \tag{4}$$

where p is the sum of the ion and electron pressure laws. Assuming isentropic laws, it is given by $p(n) = p_{\mathrm{i}}(n) + p_{\mathrm{e}}(n) = C_{\mathrm{i}}n^{\gamma_{\mathrm{i}}} + C_{\mathrm{e}}n^{\gamma_{\mathrm{e}}}$ where $C_{\mathrm{i}} > 0$ and $C_{\mathrm{e}} > 0$ are given constants and γ_{i} and γ_{e} are, respectively, the ionic and electronic ratios of specific heats. Note that it is possible to extend this model to the full Euler system like in [14], but for simplicity, we only consider isentropic laws.

We suppose that initially the domain is devoid of plasma then $\Omega_{\mathrm{P}}(0) = \emptyset$ and the associated boundary conditions are the following:

– at the cathode, we inject a quasi-neutral plasma with a normal velocity:

$$n_{|\Gamma_{\mathrm{K}}} = n_0 > 0, \quad \mathbf{u}_{|\Gamma_{\mathrm{K}}} = -u_0 v, \tag{5}$$

where v is the unit normal to Γ_{K} external to Ω and n_0 and u_0 are given positive real numbers.

– at the interface $\Gamma(t)$, following [12], we impose the value of the pressure. This pressure is the pressure reaction force exerted by the beam region on the plasma region. Using Rankine–Hugoniot relations (see [12] or [39] for more details), we obtain

$$p(x,y,t) = m_{\mathrm{e}}\frac{|j_+(x,y,t)\cdot v(x,y,t)|^2}{n_-(x,y,t)} + p_{\mathrm{e}}(n_-(x,y,t)), \tag{6}$$

for all $t > 0$ and all $(x,y) \in \Gamma(t)$. The vector v is the unit normal to $\Gamma(t)$ external to Ω_{P}, j_+ is the beam current and n_- the quasi-neutral density at the considered point:

$$j_+(x,y,t) = \lim_{\substack{(x',y')\to(x,y)\\(x',y')\in\Omega_{\mathrm{B}}}} -(n_{\mathrm{e}}\mathbf{u}_{\mathrm{e}})(x',y',t), \quad n_-(x,y,t) = \lim_{\substack{(x',y')\to(x,y)\\(x',y')\in\Omega_{\mathrm{P}}}} n(x',y',t). \tag{7}$$

2.3. The simplified Child–Langmuir model in the beam region

In the beam region there is no more ion and a quasi-neutral model cannot be valid. In [10,12,13] it is shown that the Child–Langmuir model is well adapted to describe the beam region. It is written for all $t > 0$ in the domain $\Omega_{\mathrm{B}}(t)$

$$\nabla\cdot(n_{\mathrm{e}}\mathbf{u}_{\mathrm{e}}) = 0, \quad m_{\mathrm{e}}(\mathbf{u}_{\mathrm{e}}\cdot\nabla)\mathbf{u}_{\mathrm{e}} = e\nabla\phi, \quad -\varepsilon_0\Delta\phi = -en_{\mathrm{e}}, \tag{8}$$

where e is the elementary charge and ε_0 is the vacuum permittivity. For the boundary conditions, we impose the anode potential and we suppose that the electrons leave the domain freely through the artificial boundary. At the plasma–beam interface, we assume a zero potential, using the continuity of ϕ ($\phi = 0$ in Ω_{P}). Furthermore, in the beam region electrons are accelerated by the high positive potential of the anode. This gives an electronic plasma velocity negligible compared to the electronic beam velocity. Then we impose a zero electronic velocity (in the beam's scale) at the interface. Finally, we assume a zero electric potential, this corresponds to a maximal current emission regime (see [16]). The boundary conditions are the following:

$$\begin{aligned}
&\phi_{|\Gamma_{\mathrm{A}}} = \phi_{\mathrm{A}}, \quad \nabla n_{\mathrm{e}}\cdot v_{|\Gamma_{\mathrm{art}}} = 0, \quad \nabla\mathbf{u}_{\mathrm{e}}\cdot v_{|\Gamma_{\mathrm{art}}} = 0,\\
&\nabla\phi\cdot v_{|\Gamma_{\mathrm{art}}} = 0, \quad \mathbf{u}_{\mathrm{e}|\Gamma(t)} = 0, \quad \phi_{|\Gamma(t)} = 0, \quad \nabla\phi\cdot v_{|\Gamma(t)} = 0.
\end{aligned} \tag{9}$$

Let us note that the boundary condition $\nabla\phi\cdot v_{|\Gamma(t)} = 0$ implicitly specifies the current in the direction orthogonal to the interface: $-n_{\mathrm{e}}\mathbf{u}_{\mathrm{e}}\cdot v$. This condition is called, in physics literature, the "space charge limitation condition". This expresses that the emitted current, here in the beam, is limited by the space charge. The microscopic process is such that when too much electrons are emitted in the beam, there is an accumulation of charges near the interface. This charge accumulation creates a local potential which repels the emitted elec-

trons in the plasma and so limits the emitted current. Next, these accumulated charges are accelerated by the anode potential letting other electrons leave the plasma, see [31].

In the one-dimensional case, the solution is explicit, it is given in [16]. In the multi-dimensional cases, we do not have an analytic expression for the current. It depends on the localization of the emission point on the curve $\Gamma(t)$ and on the geometry of the device. Therefore, to compute the current we need to solve the problem (8), (9). Several numerical schemes have been developed for Child–Langmuir problems, see for example [17,20] or [57] in the kinetic case. The cost is quite heavy, since the current is implicitly determined by the boundary condition: $\nabla\phi \cdot v_{|\Gamma} = 0$, with ϕ given by the resolution of the Poisson equation. We recall that our main goal is the numerical resolution of the free boundary problem related to the evolution of the plasma region. Then in order to focus on this difficulty, we prefer use a simplified model for the beam region. It is based on the one-dimensional Child–Langmuir solution. So, we first recall this solution.

In the one-dimensional case the device is delimited by the cathode, located at $x = 0$ and the anode, located at $x = 1$ then $\phi_A = \phi(1) > 0$. The interface is a moving point, we denote by $X(t)$ its position at time t. In [16], the authors show that for all $t > 0$, there exists a unique solution to system (8), (9) in one dimension, if and only if $\partial_x\phi(X(t)) \in [0, \phi_A/(1 - X(t))]$. In this case the current $n_e\mathbf{u}_e$ is in $[0, j_{CL}]$ where the maximal current value j_{CL} corresponds to $\partial_x\phi(X(t)) = 0$ and is given by

$$j_{CL}(t) = \frac{4\sqrt{2}\varepsilon_0\phi_A^{3/2}}{9\sqrt{em_e}(1 - X(t))^2}.$$

Let us note that the current is a constant of x and depends only on the potential of the anode and on the distance covered by an electron emitted from the interface to the anode.

In our two-dimensional model, we are interested in the current value at each point of the interface. Then we approximate this value assuming that a one-dimensional Child–Langmuir law can be applied on each trajectory of an electron emitted from the interface Γ. Let us consider an electron emitted from the point (x, y) of the interface $\Gamma(t)$ to the anode, we denote by (x_A, y_A) its arrival point (which must be precised) on the anode Γ_A. We approximate the current in the normal direction by the one-dimensional formula:

$$(-j_+ \cdot \nu)(x, y, t) = (n_e\mathbf{u}_e \cdot \nu)(x, y, t) \approx j_{CL}(x, y, t, d) = \frac{4\sqrt{2}\varepsilon_0(\phi_A(x_A, y_A, t))^{3/2}}{9\sqrt{em_e}d(x, y, t, \nu)^2}, \tag{10}$$

for all $(x, y) \in \Gamma(t)$ and all $t \geqslant 0$ and where $d(x, y, t, \nu)$ is the distance covered by the emitted electron from $(x, y) \in \Gamma(t)$ to the anode Γ_A. Now it remains to evaluate this distance. To this aim, we introduce the circle tangential on the one hand to the normal ν to $\Gamma(t)$ and on the other hand to the normal ν_A to Γ_A. Let $t > 0$ and $(x, y) \in \Gamma(t)$ be the starting point of the electron. Let us assume that we know the normal to $\Gamma(t)$ at this point $\nu(x, y) = (\nu_x, \nu_y)$. We denote by (x_A, y_A) its arrival point on the anode, which is unknown at this level. The unit normal to Γ_A, external to Ω, at the point (x_A, y_A) is given by $\nu_A(x_A, y_A) = 1/\sqrt{1 + f_A'(y_A)^2}(1, -f_A'(y_A))$. Finally, we denote by (x_c, y_c) the center of the circle tangential to $\nu(x, y)$ and to $\nu_A(x_A, y_A)$ (see Fig. 2).

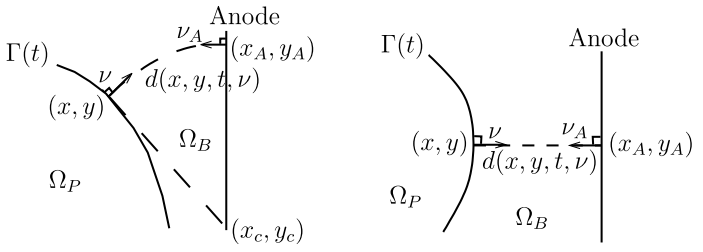

Fig. 2. Approximation of the electron trajectory in the simplified Child–Langmuir model for the beam region.

Then (x_A, y_A, x_c, y_c) is solution to the system

$$\begin{aligned} &(x_c - x)v_x + (y_c - y)v_y = 0,\\ &(x_c - x_A) - f'_A(y_A)(y_c - y_A) = 0,\\ &x_A = f_A(y_A),\\ &(x_c - x)^2 + (y_c - y)^2 = (x_c - x_A)^2 + (y_c - y_A)^2. \end{aligned} \tag{11}$$

If there exists a solution to the system (11), we assume that the electrons emitted from the point $(x, y) \in \Gamma(t)$ move along the circle of radius $\sqrt{|x_c - x|^2 + |y_c - y|^2}$ and of center (x_c, y_c). But, if the system (11) has no solution then we suppose that the electrons emitted from the point $(x, y) \in \Gamma(t)$ move along the line with direction $v(x, y)$ (see Fig. 2).

We set

$$d(x, y, t, v) = \begin{cases} \sqrt{(x - x_c)^2 + (y - y_c)^2}(\pi - \arccos(v_A \cdot v)) & \text{if (11) has a solution,}\\ \sqrt{(x - x_A)^2 + (y - y_A)^2} & \text{otherwise.} \end{cases} \tag{12}$$

This concludes the presentation of the two-dimensional asymptotic model, we summarize it in the next section.

2.4. Summary of the asymptotic model

The asymptotic model consists in the isentropic Euler system (4) for all $(x, y) \in \Omega_P(t)$ and all $t \geqslant 0$. The domain $\Omega_P(t)$ is defined by (1) and its dynamic by (3). The boundary conditions at the cathode Γ_K (see Fig. 1 for the definition of Γ_K) are given by (5) and at the plasma–beam interface by (6), (7). This system is coupled to the beam region through a boundary condition at the plasma–beam interface. The pressure (6) depends on the current in the beam region, this current is given by (10), (12) and (11).

3. The numerical method

In this section, we propose a numerical method for the discretization of the asymptotic model in the plasma region summarized in Section 2.4.

In order to track the interface, we use a volume of fluid method (see [26,59]). This is an Eulerian method which only requires the knowledge of the volume fraction of fluid present in each cell of the mesh. Then we transport the averaged quantities (on each cell of the mesh) using a Lagrange-projection scheme coupled with the SLIC algorithm (for simple line interface calculation, see [36]). The key point consists in taking account of the reaction-pressure term (6) at a discrete level.

3.1. Principle of the method

For clarity, we consider a rectangular domain, but it is possible to work with more general domain. We cover the domain Ω with a uniform rectangular mesh of size $\Delta x \times \Delta y$. For $i = 1, \ldots, K_x$ and $j = 1, \ldots, K_y$, we denote by $C_{i,j}$ the cell $[x_{i-1/2}, x_{i+1/2}) \times [y_{j-1/2}, y_{j+1/2})$ where $x_{i+1/2} = i\Delta x$ and $y_{j+1/2} = j\Delta y$. Furthermore, let $0 = t^0 < t^1 < \cdots < t^s < \cdots$ a sequence of positive real numbers, we define the time step by $\Delta t^s = t^{s+1} - t^s$ for all $s \geqslant 0$. This time step is calculated such that the classical CFL (Courant–Friedrichs–Levy) condition is satisfied (see [32]).

It is important to note that at time t^s, there are three different states for a given cell. The cell can be completely filled by the plasma. In this case it is included in the plasma region $\Omega_P(t^s)$ and it is called "full" cell. The cell can be completely filled by the beam then it is empty of plasma and completely included in the beam region $\Omega_B(t^s)$. In this case the cell is called "empty" cell. Finally, the cell can contain both plasma and vacuum then it contains a piece of the plasma–beam interface $\Gamma(t^s)$. In this case, it is called "mixed" cell. In a volume of fluid method we deal only with averaged quantities (here the averaged density and momentum) in each cells of the mesh even if they are mixed. But in order to reconstruct physical quantities, we keep the physical volume filled by the plasma in each cell.

Thus, the discrete unknowns are the discrete averaged density and velocity: $n_{i,j}^s$ and $\mathbf{u}_{i,j}^s = (u,v)_{i,j}^s$ and the discrete physical volume filled by the plasma $V_{i,j}^{\varphi,s}$ in all cell $C_{i,j}$ and at all time t^s for $i = 1,\ldots,K_x$, $j = 1,\ldots,K_y$ and $s \in \mathbb{N}$. The physical quantities, $n_{i,j}^{\varphi,s}$ and $\mathbf{u}_{i,j}^{\varphi,s}$, are given conserving the mass and the momentum

$$n_{i,j}^{\varphi,s} = \frac{\Delta x \Delta y}{V_{i,j}^{\varphi,s}}\, n_{i,j}^s \quad \text{and} \quad \mathbf{u}_{i,j}^{\varphi,s} = \mathbf{u}_{i,j}^s. \tag{13}$$

A time step of the discretization consists in the determination of all the averaged quantities and the physical volume filled by the plasma at the discrete time t^{s+1} ($n_{i,j}^{s+1}$, $\mathbf{u}_{i,j}^{s+1}$ and $V_{i,j}^{\varphi,s+1}$ for all $i = 1,\ldots,K_x$ and all $j = 1,\ldots,K_y$) knowing these quantities at the discrete time t^s. To this aim, we split the isentropic Euler system (4) in the following two systems

$$(S_x)\begin{cases} \partial_t n + \partial_x(nu) = 0, \\ \partial_t(n\mathbf{u}) + \partial_x(nu\mathbf{u}) + \begin{pmatrix} \frac{\partial_x p}{m_i+m_e} \\ 0 \end{pmatrix} = 0, \end{cases} \quad (S_y)\begin{cases} \partial_t n + \partial_y(nv) = 0, \\ \partial_t(n\mathbf{u}) + \partial_y(nv\mathbf{u}) + \begin{pmatrix} 0 \\ \frac{\partial_y p}{m_i+m_e} \end{pmatrix} = 0, \end{cases} \tag{14}$$

where $\mathbf{u} = (u,v)$ and with the boundary conditions (5), (6), (7) and (10).

We solve the system (S_x) of (14) using a Lagrange-projection scheme, this gives the approximate variables $n_{i,j}^{s+1/2}$, $\mathbf{u}_{i,j}^{s+1/2}$ and $V_{i,j}^{\varphi,s+1/2}$. Then, we use these values for the initial condition of the system (S_y) of (14) which is solved still using a Lagrange-projection scheme. We obtain the approximate variables $n_{i,j}^{s+1}$, $\mathbf{u}_{i,j}^{s+1}$ and $V_{i,j}^{\varphi,s+1}$ at time t^{s+1}. In order to not privilege a direction, during the next time step we begin solving (S_y) and finish with (S_x).

The Lagrange-projection scheme consists in two steps: the Lagrangian step and the projection step. During the Lagrangian step, we transport the density and the velocity following the characteristic curves of the considered system. During the projection step, we distribute the transported quantities on the Eulerian grid $\{C_{i,j}; i = 1,\ldots,K_x, j = 1,\ldots,K_y\}$. We detail these two steps for the system (S_x) of (14) in the following.

3.2. The Lagrangian step in the x direction

We recall that the system S_x of (14) holds only in the domain $\Omega_P(t)$ for all $t > 0$. Then this step only concerns full or mixed cells. Furthermore we have to take into account of the boundary condition (6) at the plasma–beam interface. Thus, we must localize the (full or mixed) cells for which we use this boundary condition. We call these cells "border cells" and the other full or mixed cells "internal cells" due to their geometric relation with the plasma region. We begin this step with the location of border and internal cells. Let $s \geqslant 0$, we define

$$\mathscr{E}_x^s = \{C_{i_0,j},\ \text{where } j \in \{1,\ldots,K_y\} \text{ and } i_0 = \max\{i \in \{1,\ldots,K_x\}/n_{i,j}^s > 0\}\},$$
$$\mathscr{E}_y^s = \{C_{i,j_0},\ \text{where } i \in \{1,\ldots,K_x\} \text{ and } j_0 = \max\{j \in \{1,\ldots,K_y\}/n_{i,j}^s > 0\}\}.$$

The set $\Gamma_{\text{num}}^s = \mathscr{E}_x^s \cup \mathscr{E}_y^s$ contains the border cells and gives a diffusive approximation of the interface as shown in Fig. 3 where the cells included in Γ_{num}^s are located by a point.

Then, the cells $C_{i,j}$ of the mesh sucah that $C_{i,j} \notin \Gamma_{\text{num}}^s$ and such that $n_{i,j}^s > 0$, are the internal cells. These cells are located by a cross in Fig. 3.

We begin with the presentation of the Lagrangian step for internal cells, then we present it for the border cells taking into account of the pressure reaction force.

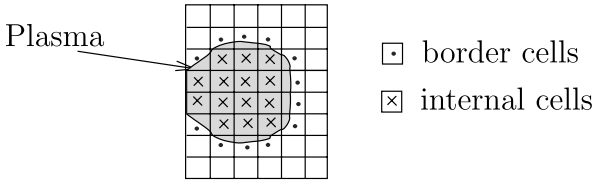

Fig. 3. Location of border cells for which we have to take into account of the pressure reaction force in the discretization.

3.2.1. The Lagrangian step in the x direction for internal cells

Let $s \in \mathbb{N}$ be fixed, we introduce the Lagrangian coordinates at time t^s associated to system S_x of (14) (see [46]). We denote by $X(t;x,y,t^s)$ the characteristic curve at time t such that $X(t^s;x,y,t^s) = x$ for all y. Then, for all internal cell $C_{i,j}$ with $j = 1,\dots,K_y$ and $i \in \{1,\dots,K_x\}$, we denote by $X^{s+1}_{i+1/2,j}$ and $X^{s+1}_{i-1/2,j}$, approximations of $X(t^{s+1};x_{i+1/2},y_j,t^s)$ and $X(t^{s+1};x_{i-1/2},y_j,t^s)$. They are given using an explicit Euler scheme:

$$X^{s+1}_{k+1/2,j} = x_{k+1/2} + \Delta t^s u^s_{k+1/2,j} \quad \text{for } k = i \text{ or } i-1, \tag{15}$$

and where $u^s_{k+1/2,j}$ is an approximation of $u(x_{k+1/2},y_j,t^s)$. Classically, $u^s_{k+1/2,j}$ is determined using an approximate solution of the following Riemann problem in Lagrangian coordinates:

$$\begin{aligned} &\partial_t \tau - \partial_m u = 0,\\ &(m_i + m_e)\partial_t u + \partial_m p = 0,\\ &(\tau,u)(m,t=0) = \begin{cases} (1/n^s_{k,j}, u^s_{k,j}) & \text{if } m < 0,\\ (1/n^s_{k+1,j}, u^s_{k+1,j}) & \text{if } m > 0, \end{cases} \end{aligned} \tag{16}$$

where $\tau = 1/n$ is the specific volume and the mass variable is defined by $\mathrm{d}m = n\,\mathrm{d}x$. Here, we use the polynomial upwind scheme (see [15] or [10], this is a Roe type solver) in order to determine this approximate solution.

Then, for all internal Eulerian cell $C_{i,j} = [x_{i-1/2},x_{i+1/2}) \times [y_{j-1/2},y_{j+1/2})$ we define an associated Lagrangian cell $\tilde{C}^{s+1/2}_{i,j} = [X^{s+1}_{i-1/2,j}, X^{s+1}_{i+1/2,j}) \times [y_{j-1/2},y_{j+1/2})$. We associate to $\tilde{C}^{s+1/2}_{i,j}$ the approximate values of the averaged density and velocity on this cell, denoted by $\tilde{n}^{s+1/2}_{i,j}$ and $(\tilde{u}^{s+1/2}_{i,j}, \tilde{v}^{s+1/2}_{i,j})$. Using the Lagrangian coordinates, we have

$$\begin{aligned} &\left(X^{s+1}_{i+1/2,j} - X^{s+1}_{i-1/2,j}\right)\tilde{n}^{s+1/2}_{i,j} = \Delta x n^s_{i,j},\\ &\tilde{u}^{s+1/2}_{i,j} = u^s_{i,j} - \frac{\Delta t^s}{\Delta x n^s_{i,j}(m_i + m_e)}\left(p^s_{i+1/2,j} - p^s_{i-1/2,j}\right),\\ &\tilde{v}^{s+1/2}_{i,j} = v^s_{i,j}, \end{aligned} \tag{17}$$

where the pressure terms $p^s_{i+1/2,j}$ and $p^s_{i-1/2,j}$ are calculated with the approximate solutions of the Riemann problem (16) given by the polynomial upwind scheme (see [15] or [10]), respectively for $k = i$ and $i-1$.

3.2.2. The Lagrangian step in the x direction for border cells

Let $C_{i,j} \in \Gamma^s_{\mathrm{num}}$ be a border cell, the principle of the scheme is the same. We introduce the associated Lagrangian cell $\tilde{C}^{s+1/2}_{i,j} = [X^{s+1}_{i-1/2,j}, X^{s+1}_{i+1/2,j}) \times [y_{j-1/2},y_{j+1/2})$ where $X^{s+1}_{i-1/2,j}$ and $X^{s+1}_{i+1/2,j}$ are given by (15). The transported averaged quantities on the Lagrangian cell, $\tilde{n}^{s+1/2}_{i,j}$ and $(\tilde{u}^{s+1/2}_{i,j}, \tilde{v}^{s+1/2}_{i,j})$ are given by (17). It remains to precise the velocity and the pressure between the two cells: $(u^s_{k+1/2,j}, p^s_{k+1/2,j})$ for $k = i$ and $i-1$. Let $k = i$ or $i-1$, if $C_{k,j}$ and $C_{k+1,j}$ are mixed or full cells, i.e. if $n^s_{k,j} \neq 0$ and $n^s_{k+1,j} \neq 0$ then the flux $(u^s_{k+1/2,j}, p^s_{k+1/2,j})$ is given by the polynomial upwind scheme applied to the Riemann problem (16). Otherwise, $C_{i-1,j}$ (or/and $C_{i+1,j}$) is an empty cell. Let us assume without loss of generality that $C_{i+1,j}$ is empty, the other cases can be easily deduced. In this case, the boundary condition (6) gives the pressure law on the plasma–beam interface. First, let us assume that we know an approximation $p^s_{i,j}$ of this pressure law on $\Gamma^s_{i,j} = \Gamma(t^s) \cap C_{i,j}$: the part of the plasma–beam interface included in $C_{i,j}$ and we suppose that we know an approximation of the outward unit normal vector to $\Gamma^s_{i,j}$: $v^s_{i,j}$. We will see in the following our choice for $p^s_{i,j}$ and $v^s_{i,j}$. Then, we set $p^s_{i+1/2,j} = p^s_{i,j} v^s_{i,j} \cdot (1,0)$. It remains to determine $u^s_{i+1/2,j}$. Since $n^s_{i+1,j} = 0$, we can no more work with Lagrangian coordinates, then we introduce the following Riemann problem between fluid and "pseudo-vacuum" with a non zero pressure:

$$\begin{aligned} &\partial_t n + \partial_x(nu) = 0,\\ &(m_i + m_e)(\partial_t(nu) + \partial_x(nu^2)_x) + \partial_x p = 0,\\ &\begin{cases} (n,u) = (n^{\varphi,s}_{i,j}, u^{\varphi,s}_{i,j}), & \text{if } x < 0,\\ (n,p) = (0, p^s_{i,j} v^s_{i,j} \cdot (1,0)), & \text{if } x > 0. \end{cases} \end{aligned}$$

where $n_{i,j}^{\varphi,s}$ and $u_{i,j}^{\varphi,s}$ are the physical quantities in the cell $C_{i,j}$ at time t^s. Let us note that $p_{i,j}^s v_{i,j}^s \cdot (1,0)$ is the projection on the line $\{y = 0\}$ of the pressure force. It corresponds to the part of this force acting during the Lagrangian step in the x-direction.

Classically, if $p_{i,j}^s = 0$ the solution is given by a rarefaction wave separating the left state $(n_{i,j}^{\varphi,s}, u_{i,j}^{\varphi,s})$ and the vacuum (see [46]). This wave is associated to the first eigen value $\lambda_- = u - c$ where c is the sound speed given by $c = \sqrt{p'(n)/(m_\mathrm{i} + m_\mathrm{e})}$. In this case, the velocity of the plasma–vacuum interface is given by

$$u_{i+1/2,j}^s = u_{i,j}^{\varphi,s} + \frac{2}{\gamma - 1}\sqrt{\frac{p'(n_{i,j}^{\varphi,s})}{m_\mathrm{i} + m_\mathrm{e}}}.$$

If $p_{i,j}^s \neq 0$ we can prove (see [39] for details) that there is a unique solution constituted of three constant states $(n_{i,j}^{\varphi,s}, u_{k,j}^{\varphi,s})$, (n_I, u_I) and the "pseudo-vacuum" such that (n_I, u_I) and the "pseudo-vacuum" are separated by a shock wave of velocity $\sigma = u_I$. Furthermore $n_I = p^{-1}(p_{i,j}^s v_{i,j}^s \cdot (1,0))$ and

– if $n_I > n_{i,j}^{\varphi,s}$ then $(n_{i,j}^{\varphi,s}, u_{i,j}^{\varphi,s})$ and (n_I, u_I) are separated by a shock wave associated to the first eigen value $\lambda_- = u - c$ and

$$u_I = u_{i,j}^{\varphi,s} - \frac{n_I - n_{i,j}^{\varphi,s}}{\sqrt{n_I n_{i,j}^{\varphi,s}}}\sqrt{\frac{p(n_I) - p(n_{i,j}^{\varphi,s})}{(m_\mathrm{i} + m_\mathrm{e})(n_I - n_{i,j}^{\varphi,s})}},$$

– otherwise $(n_{i,j}^{\varphi,s}, u_{i,j}^{\varphi,s})$ and (n_I, u_I) are separated by a rarefaction wave associated to the first eigen value $\lambda_- = u - c$ and

$$u_I = u_{i,j}^{\varphi,s} + \frac{2}{\gamma - 1}\left(\sqrt{\frac{p'(n_{i,j}^{\varphi,s})}{m_\mathrm{i} + m_\mathrm{e}}} - \sqrt{\frac{p'(n_I)}{m_\mathrm{i} + m_\mathrm{e}}}\right).$$

In both cases, we set

$$u_{i+1/2,j}^s = u_I.$$

It remains to calculate $p_{i,j}^s$ and $v_{i,j}^s$ the approximations of the reaction-pressure law on $\Gamma_{i,j}^s = \Gamma(t^s) \cap C_{i,j}$: the part of the plasma–beam interface included in $C_{i,j}$ and of the outward unit normal vector to $\Gamma_{i,j}^s$.

3.2.2.1. Approximation of the unit normal and of the pressure reaction force. We begin with the reconstruction of the outward unit normal vector to $\Gamma_{i,j}^s$. We use Youngs' method detailed in [60]. This is a volume of fluids method which directly gives an oblique representation of the 2D interface. We stress that we use this method only for the calculation of the unit normal but not for the projection step. For the projection step, we use the SLIC method which rather defines transfer priorities between the different fluids. Youngs' method consists in reconstructing the slope of the interface in each mixed cell from the associated normal vector. We briefly recall the principle of this method in the following.

For all cells neighboring $C_{i,j}$, i.e. the cells $C_{k,l}$ with $(k,l) \in \{i-1, i, i+1\} \times \{j-1, j, j+1\}$ and $(k,l) \neq (i,j)$, we compute the associated volume fraction filled by the plasma at time t^s : $f_{k,l}^s = V_{k,l}^{\varphi,s}/\Delta x \times \Delta y$. We recall that $V_{k,l}^{\varphi,s}$ is the physical volume filled by the plasma in the cell $C_{k,l}$ at time t^s. We deduce the volume fractions corresponding to each direction: f_E^s, f_W^s, f_N^s and f_S^s, we get

$$f_\mathrm{N}^s = \frac{f_{i-1,j+1}^s + 2f_{i,j+1}^s + f_{i+1,j+1}^s}{4}, \quad f_\mathrm{S}^s = \frac{f_{i-1,j-1}^s + 2f_{i,j-1}^s + f_{i+1,j-1}^s}{4},$$
$$f_\mathrm{E}^s = \frac{f_{i+1,j-1}^s + 2f_{i+1,j}^s + f_{i+1,j+1}^s}{4}, \quad f_\mathrm{W}^s = \frac{f_{i-1,j-1}^s + 2f_{i-1,j}^s + f_{i-1,j+1}^s}{4}.$$

The outward unit normal to the interface on the cell $C_{i,j}$ is then deduced from the approximated gradient of $f_{i,j}^s$: $\nabla_\mathrm{app} f_{i,j}^s = (\frac{f_\mathrm{E}^s - f_\mathrm{W}^s}{2\Delta x}, \frac{f_\mathrm{N}^s - f_\mathrm{S}^s}{2\Delta y})$ by setting $v_{i,j}^s = \frac{-\nabla_\mathrm{app} f_{i,j}^s}{\|\nabla_\mathrm{app} f_{i,j}^s\|}$.

Now let us turn to $p^s_{i,j}$, the approximation of the reaction-pressure on $\Gamma^s_{i,j}$. Using (12), we determine the approximate distance $d^s_{i,j}$ covered by an electron emitted from the center of $C_{i,j}$, we set $d^s_{i,j} = d(x_i, y_j, t^s, v^s_{i,j})$ with $x_i = (i-1/2)\Delta x$ and $y_j = (j-1/2)\Delta y$. Inserting the result in (10), we obtain an approximation of the emitted current in the plasma in the normal direction $j^s_{\mathrm{CL},i,j} = j_{\mathrm{CL}}(x_i, y_j, t^s, d^s_{i,j})$. Thanks to (6), we obtain the approximate reaction-pressure exerted on the plasma–beam interface in the cell $C_{i,j}$ at time t^s:

$$p^s_{i,j} = m_{\mathrm{e}} \frac{|j^s_{\mathrm{CL},i,j}|^2}{n^{\varphi,s}_{i,j}} + p_{\mathrm{e}}(n^{\varphi,s}_{i,j}),$$

where $n^{\varphi,s}_{i,j}$ is the physical density of the plasma in the cell $C_{i,j}$ at time t^s defined by (13).

This concludes the presentation of the Lagrangian step, during which we transport the quantities along the characteristic curves. It remains to project these transported quantities on the fixed Eulerian mesh. We do it in the next section.

3.3. The projection step in the x direction

During the Lagrangian step in the x-direction the averaged quantities have been advected following characteristic curves. Here projecting these quantities, we go back to the initial Eulerian fixed grid.

3.3.1. Principle of the method

Let us consider the Eulerian cell $C_{i,j}$ with $i = 1, \ldots, K_x$ and $j = 1, \ldots, K_y$. After the Lagrangian step in the x-direction, we know the averaged density, $\tilde{n}^{s+1/2}_{i,j}$, and the mean velocity, $(\tilde{u}^{s+1/2}_{i,j}, \tilde{v}^{s+1/2}_{i,j})$, in the Lagrangian cell $\tilde{C}^{s+1/2}_{i,j} = [X^{s+1}_{i-1/2,j}, X^{s+1}_{i+1/2,j}) \times [y_{j-1/2}, y_{j+1/2})$ associated to $C_{i,j}$. We recall that $X^{s+1}_{i-1/2,j}$ and $X^{s+1}_{i+1/2,j}$ are defined by (15). During the projection step in the x direction, we first determine physical quantities in the Lagrangian cell $\tilde{C}^{s+1/2}_{i,j}$ then we project them on the Eulerian grid.

We define the physical quantities on the Lagrangian cell, assuming the deformation of the physical volume $V^{\varphi,s}_{i,j}$ proportional to the deformation of $C_{i,j}$. Then the physical volume filled by the plasma in $\tilde{C}^{s+1/2}_{i,j}$ at time t^{s+1} is given by

$$\tilde{V}^{\varphi,s+1/2}_{i,j} = V^{\varphi,s}_{i,j} \frac{\tilde{V}^{s+1/2}_{i,j}}{\Delta x \Delta y}, \tag{18}$$

where $\tilde{V}^{s+1/2}_{i,j} = (X^{s+1}_{i+1/2,j} - X^{s+1}_{i-1/2,j})\Delta y$ is the volume of the Lagrangian cell $\tilde{C}^{s+1/2}_{i,j}$. This gives the physical density and velocity of the plasma in the cell $\tilde{C}^{s+1/2}_{i,j}$ after the Lagrangian step in the x-direction

$$\tilde{n}^{\varphi,s+1/2}_{i,j} = \frac{\tilde{V}^{s+1/2}_{i,j}}{\tilde{V}^{\varphi,s+1/2}_{i,j}} \tilde{n}^{s+1/2}_{i,j}, \quad \tilde{u}^{\varphi,s+1/2}_{i,j} = \tilde{u}^{s+1/2}_{i,j}, \quad \tilde{v}^{\varphi,s+1/2}_{i,j} = \tilde{v}^{s+1/2}_{i,j}.$$

We want to project these quantities and obtain the averaged density and velocity in the Euler cell $C_{i,j}$ at time $t^{s+1/2}$ (i.e. before the Lagrange-projection step in the y-direction).

We denote by $\sigma_{i+1/2,j}$ the interface between $C_{i,j}$ and $C_{i+1,j}$ and by $V^{\varphi,s+1/2}_{i+1/2,j}$ the signed physical volume of plasma which crosses $\sigma_{i+1/2,j}$ between the times t^s and t^{s+1} during the previous Lagrangian step in the x-direction. This volume is positive if the plasma is going from $C_{i,j}$ to $C_{i+1,j}$ and negative otherwise. Similarly, we denote by $V^{\varphi,s+1/2}_{i-1/2,j}$ the signed physical volume of plasma which crosses $\sigma_{i-1/2,j}$, the interface between $C_{i-1,j}$ and $C_{i,j}$, during the same time. These quantities will be precised later.

Then the unknowns at time $t^{s+1/2}$ are given by

$$\begin{aligned}
V^{\varphi,s+1/2}_{i,j} &= V^{\varphi,s}_{i,j} - V^{\varphi,s+1/2}_{i+1/2,j} + V^{\varphi,s+1/2}_{i-1/2,j},\\
V_{i,j} n^{s+1/2}_{i,j} &= \tilde{V}^{\varphi,s+1/2}_{i,j} \tilde{n}^{\varphi,s+1/2}_{i,j} - V^{\varphi,s+1/2}_{i+1/2,j} \tilde{n}^{\varphi,s+1/2}_{i+1/2,j} + V^{\varphi,s+1/2}_{i-1/2,j} \tilde{n}^{\varphi,s+1/2}_{i-1/2,j},\\
V_{i,j} (nu)^{s+1/2}_{i,j} &= \tilde{V}^{\varphi,s+1/2}_{i,j} (\tilde{n}\tilde{u})^{\varphi,s+1/2}_{i,j} - V^{\varphi,s+1/2}_{i+1/2,j} (\tilde{n}\tilde{u})^{\varphi,s+1/2}_{i+1/2,j} + V^{\varphi,s+1/2}_{i-1/2,j} (\tilde{n}\tilde{u})^{\varphi,s+1/2}_{i-1/2,j},\\
V_{i,j} (nv)^{s+1/2}_{i,j} &= \tilde{V}^{\varphi,s+1/2}_{i,j} (\tilde{n}\tilde{v})^{\varphi,s+1/2}_{i,j} - V^{\varphi,s+1/2}_{i+1/2,j} (\tilde{n}\tilde{v})^{\varphi,s+1/2}_{i+1/2,j} + V^{\varphi,s+1/2}_{i-1/2,j} (\tilde{n}\tilde{v})^{\varphi,s+1/2}_{i-1/2,j},
\end{aligned}$$

where for $l = i - 1$ or i

$$(\tilde{n}, \tilde{u}, \tilde{v})^{\varphi,s+1/2}_{l+1/2,j} = \begin{cases} (\tilde{n}, \tilde{u}, \tilde{v})^{\varphi,s+1/2}_{l,j} & \text{if } X^{s+1}_{l+1/2,j} \geqslant x_{l+1/2}, \\ (\tilde{n}, \tilde{u}, \tilde{v})^{\varphi,s+1/2}_{l+1,j} & \text{otherwise.} \end{cases}$$

In order to conclude the presentation of the projection step, we must define the signed physical volume of plasma which crosses each interface during the Lagrangian step in the x direction, i.e. $V^{\varphi,s+1/2}_{i+1/2,j}$ for all $i = 1, \ldots, K_x$, all $j = 1, \ldots, K_y$ and all $s \geqslant 0$.

3.3.2. Determination of the physical volume flowed through two cells during Δt^s

Let $s \geqslant 0$, $i \in \{1, \ldots, K_x\}$ and $j \in \{1, \ldots, K_y\}$, we assume that $X^{s+1}_{i+1/2,j} \geqslant x_{i+1/2}$, (the case $X^{s+1}_{i+1/2,j} < x_{i+1/2}$ can be easily deduced). In this case, the plasma flowed from $C_{i,j}$ to $C_{i+1,j}$, then, the value $V^{\varphi,s+1/2}_{i+1/2,j}$ depends on the state of the cell $C_{i,j}$ at time t^s: i.e. if $C_{i,j}$ is a full or a mixed cell.

- 1st *case*: *$C_{i,j}$ is full of plasma*:
  If the cell $C_{i,j}$ is full then all its volume flowing through $\sigma_{i+1/2}$, the interface between $C_{i,j}$ and $C_{i+1,j}$, is a physical plasma volume then

$$V^{\varphi,s+1/2}_{i+1/2,j} = \left(X^{s+1}_{i+1/2,j} - x_{i+1/2}\right)\Delta y.$$

- 2nd *case*: *$C_{i,j}$ is a mixed cell*:
  If the cell $C_{i,j}$ is mixed, we must decide where was the plasma in the cell $C_{i,j}$ at time t^s as well as where is the plasma in the cell $\tilde{C}^{s+1/2}_{i,j}$ after the Lagrangian step in the x-direction. From these quantities we easily calculate the volume of plasma which has flowed from $C_{i,j}$ to $C_{i+1,j}$. We use the SLIC algorithm (simple line interface calculation) [36]. This algorithm gives a non continuous reconstruction of the plasma–vacuum interface. Then it does not give a realistic representation of the interface but it rather defines transfer priorities between fluids. The SLIC method is not limited by the number of fluids present in the problem. Here, we detail it in our particular situation with two "fluids": the plasma and the vacuum.

  In the SLIC method, the priorities of transfer in a cell $C_{i,j}$ depends on the state of its neighbors $C_{i-1,j}$ and $C_{i+1,j}$. Each cell can be full, mixed or empty and so nine different cases have to be considered.

– *First case:* $C_{i-1,j}$ and $C_{i+1,j}$ are both empty. In this case, we assume that the plasma is located at the center of the cell $C_{i,j}$. In all cases, the plasma in the cell $\tilde{C}^{s+1/2}_{i,j}$ is located like in the cell $C_{i,j}$. The situation is drawn in Figs. 4 and 5a.
  An easy calculation shows that the physical plasma volume of $C_{i,j}$ flowed through $\sigma_{i+1/2,j}$ is given by

$$V^{\varphi,s+1/2}_{i+1/2,j} = \min\left(V^{s+1/2}_{i+1/2,j} - \min\left(V^{s+1/2}_{i+1/2,j}; \left(\tilde{V}^{s+1/2}_{i,j} - \tilde{V}^{\varphi,s+1/2}_{i,j}\right)/2\right); \tilde{V}^{\varphi,s+1/2}_{i,j}\right),$$

  where $V^{s}_{i+1/2,j}$, the volume of $C_{i,j}$ flowed through $\sigma_{i+1/2,j}$, is given by

$$V^{s+1/2}_{i+1/2,j} = \left(X^{s+1}_{i+1/2,j} - x_{i+1/2}\right)\Delta y. \tag{19}$$

  Furthermore $\tilde{V}^{\varphi,s+1/2}_{i,j}$, the physical volume filled by the plasma in $\tilde{C}^{s+1/2}_{i,j}$ is given by (18) and finally $\tilde{V}^{s+1/2}_{i,j}$, the volume of $\tilde{C}^{s+1/2}_{i,j}$, is given by

$$\tilde{V}^{s+1/2}_{i,j} = \left(X^{s+1}_{i+1/2,j} - X^{s+1}_{i-1/2,j}\right)\Delta y. \tag{20}$$

– *Second case:* $C_{i-1,j}$ and $C_{i+1,j}$ are both full. This case is symmetric to the previous, we assume that the vacuum is located at the center of the cells $C_{i,j}$ and $\tilde{C}^{s+1/2}_{i,j}$ with half of the plasma to the left and half of the plasma to the right (see Fig. 5b). In this case the physical plasma volume of $C_{i,j}$ flowed through $\sigma_{i+1/2,j}$ is given by

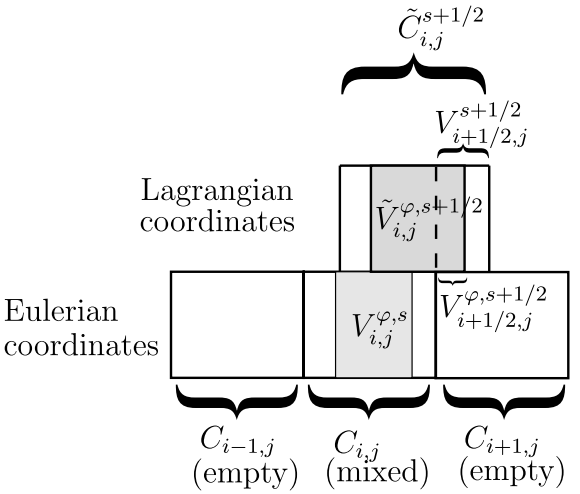

Fig. 4. Determination of the plasma volume flowed through $\sigma_{i+1/2,j} = \partial C_{i,j} \cap \partial C_{i+1,j}$ during a time step when $C_{i,j}$ is a mixed cell and $C_{i-1,j}$ and $C_{i+1,j}$ are empty cells.

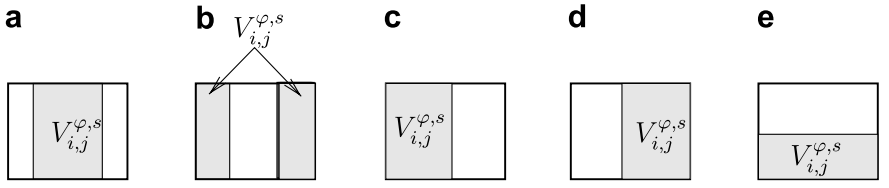

Fig. 5. Location of the plasma volume in the cell $C_{i,j}$ in the case (a) $C_{i-1,j}$ and $C_{i+1,j}$ are both empty, (b) $C_{i-1,j}$ and $C_{i+1,j}$ are both full, (c) $C_{i-1,j}$ is full and $C_{i+1,j}$ is empty or $C_{i-1,j}$ is full and $C_{i+1,j}$ is mixed or $C_{i-1,j}$ is mixed and $C_{i+1,j}$ is empty, (d) $C_{i-1,j}$ is empty and $C_{i+1,j}$ is full or $C_{i-1,j}$ is mixed and $C_{i+1,j}$ is full or $C_{i-1,j}$ is empty and $C_{i+1,j}$ is mixed, (e) $C_{i-1,j}$ and $C_{i+1,j}$ are both mixed.

$$V_{i+1/2,j}^{\varphi,s+1/2} = \min\left(V_{i+1/2,j}^{s+1/2}; \tilde{V}_{i,j}^{\varphi,s+1/2}/2\right),$$

where we recall that $\tilde{V}_{i,j}^{\varphi,s+1/2}$ and $V_{i+1/2,j}^{s+1/2}$ are given by (18) and (19).

– *Third and fourth cases:* $C_{i-1,j}$ full and $C_{i+1,j}$ empty or $C_{i-1,j}$ empty and $C_{i+1,j}$ full. We assume that the plasma is located right next to the plasma (see Figs. 5c and d). This gives

$$V_{i+1/2,j}^{\varphi,s+1/2} = \begin{cases} \min\left(V_{i+1/2,j}^{s+1/2} - \min\left(V_{i+1/2,j}^{s+1/2}; \tilde{V}_{i,j}^{s+1/2} - \tilde{V}_{i,j}^{\varphi,s+1/2}\right); \tilde{V}_{i,j}^{\varphi,s+1/2}\right) & \text{if } C_{i-1,j} \text{ is full,} \\ \min\left(V_{i+1/2,j}^{s+1/2}; \tilde{V}_{i,j}^{\varphi,s+1/2}\right) & \text{if } C_{i-1,j} \text{ is empty,} \end{cases}$$

where we recall that $\tilde{V}_{i,j}^{\varphi,s+1/2}$, $V_{i+1/2,j}^{s+1/2}$ and $\tilde{V}_{i,j}^{s+1/2}$ are respectively given by (18)–(20). Remark that the dissymmetry of these two cases is due to the positivity of the velocity.

– *Fifth and sixth cases:* $C_{i-1,j}$ full and $C_{i+1,j}$ mixed or $C_{i-1,j}$ mixed and $C_{i+1,j}$ full. The plasma is put right next to the full cell (see Figs. 5c and d). We obtain

$$V_{i+1/2,j}^{\varphi,s+1/2} = \begin{cases} \min\left(V_{i+1/2,j}^{s} - \min\left(V_{i+1/2,j}^{s}; \tilde{V}_{i,j}^{s+1/2} - \tilde{V}_{i,j}^{\varphi,s}\right); \tilde{V}_{i,j}^{\varphi,s}\right), & \text{if } C_{i-1,j} \text{ is full,} \\ \min\left(V_{i+1/2,j}^{s}; \tilde{V}_{i,j}^{\varphi,s}\right), & \text{if } C_{i-1,j} \text{ is mixed.} \end{cases}$$

– *Seventh and eighth cases:* $C_{i-1,j}$ mixed and $C_{i+1,j}$ empty or $C_{i-1,j}$ empty and $C_{i+1,j}$ mixed. We assume that the plasma is located next to the mixed cell (see Figs. 5c and d). This gives

$$V_{i+1/2,j}^{\varphi,s+1/2} = \begin{cases} \min\left(V_{i+1/2,j}^{s} - \min\left(V_{i+1/2,j}^{s}; \tilde{V}_{i,j}^{s+1/2} - \tilde{V}_{i,j}^{\varphi,s}\right); \tilde{V}_{i,j}^{\varphi,s}\right) & \text{if } C_{i-1,j} \text{ is mixed,} \\ \min(V_{i+1/2,j}^{s}; \tilde{V}_{i,j}^{\varphi,s}) & \text{if } C_{i-1,j} \text{ is empty.} \end{cases}$$

– *Ninth case:* $C_{i-1,j}$ and $C_{i+1,j}$ are both mixed. In this case we cannot privilege one cell then we consider a plasma–vacuum interface in $C_{i,j}$ parallel to the axis $[0x)$ (see Fig. 5e). We deduce

$$V^{\varphi,s+1/2}_{i+1/2,j} = \frac{\tilde{V}^{\varphi,s}_{i,j}}{\tilde{V}^{s+1/2}_{i,j}} V^{s}_{i+1/2,j}.$$

This concludes the presentation of the projection step and so the presentation of the Lagrange-projection scheme.

4. The numerical results

In this section, we first study the accuracy of the proposed numerical method. We apply it to a test case of a fluid compression for which an analytic solution is known. Next, we present numerical results for high current diodes, modeled by the quasi-neutral system (4)–(6).

4.1. Accuracy of the numerical scheme: homogeneous space pressure

We study the accuracy of the numerical scheme on a test case of a fluid compression. We assume that the problem is invariant in the $[0,z)$ direction and we consider a two-dimensional radial problem in the plane $(0,x,y)$ as shown in Fig. 6. We consider a fluid occupying initially a ball of center $0=(0,0)$ and of radius $R_0>0$ at $t=0$. This fluid is subject to a given external uniform pressure on its surface and so it is compressed on the point $(0,0)$. Let us denote by ρ and $\mathbf{u}$ the density and the two-dimensional velocity of the fluid and by $R(t)$ the radius of the ball occupied by the fluid at the time $t>0$. We will precise $R(t)$ in the following. Then, assuming an adiabatic pressure law, ρ and $\mathbf{u}$ satisfy the isentropic Euler equations

$$\begin{aligned} &\partial_t \rho + \nabla\cdot(\rho\mathbf{u}) = 0,\\ &\partial_t \mathbf{u} + \nabla\cdot(\rho\mathbf{u}\otimes\mathbf{u}) + \nabla p = 0,\\ &p(x,y,t) = \begin{cases} K\rho^{\gamma} & \text{if } x^2+y^2 < R^2(t),\\ P_{\mathrm{S}}(t) & \text{if } x^2+y^2 = R^2(t), \end{cases} \end{aligned} \tag{21}$$

for all $(x,y)\in\mathbb{R}^2$ such that $x^2+y^2\leqslant R^2(t)$ and all $t>0$. The constants $K>0$ and $\gamma>1$ are given positive real numbers defining the pressure law. Finally, P_{S} is the given external uniform pressure applied on the boundary of the domain.

In [2], it is shown that if the applied external uniform pressure and the initial conditions are well chosen then the system (21) has an analytic solution. Let us denote by $T_{\mathrm{f}}>0$ the final compression time. Then, at time T_{f} the compression on point $(0,0)$ has occurred. We set $\Omega = 1/T_{\mathrm{f}}$ the compression frequency, and we define the following radial initial condition for the density

$$\rho(x,y,0) = \rho(r\cos\theta, r\sin\theta, 0) = \begin{cases} \bar{\rho}_0 + \frac{(\gamma-1)^2\Omega^2}{2\gamma^3 K} r^{2/(\gamma-1)} & \text{if } r=\sqrt{x^2+y^2}\leqslant R_0,\\ 0 & \text{otherwise,} \end{cases}$$

where $\bar{\rho}_0>0$ is a given positive real number. The initial velocity is given by

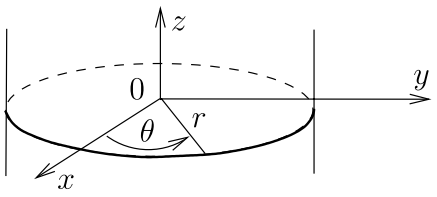

Fig. 6. Fluid subject to an external homogeneous space pressure.

$$\mathbf{u}(x,y,0) = \mathbf{u}(r\cos\theta, r\sin\theta, 0) = \begin{cases} -\frac{\Omega r}{\gamma}(\cos\theta, \sin\theta) & \text{if } r = \sqrt{x^2+y^2} \leqslant R_0, \\ (0,0) & \text{otherwise.} \end{cases}$$

The external uniform pressure applied on the boundary of the domain and the radius of the domain are defined by

$$P_S(t) = \frac{K}{(1-\Omega t)^2}\left(\bar{\rho}_0 + \frac{(\gamma-1)^2\Omega^2}{2\gamma^3 K} R_0^{2/(\gamma-1)}\right)^{\gamma}, \quad R(t) = R_0(1-\Omega t)^{1/\gamma}, \tag{22}$$

for all $t < T_f$.

In this case an analytic solution is given by

$$(\rho, \mathbf{u})(x,y,t) = (\rho,\mathbf{u})(r\cos\theta, r\sin\theta, t) = \begin{cases} (\tilde{\rho}(r,t), \tilde{u}(r,t)(\cos\theta,\sin\theta)) & \text{if } r \leqslant R(t), \\ (0,(0,0)) & \text{otherwise,} \end{cases} \tag{23}$$

where

$$\tilde{\rho}(r,t) = \frac{1}{(1-\Omega t)^{2/\gamma}}\left(\bar{\rho}_0 + \frac{(\gamma-1)^2\Omega^2}{2\gamma^3 K}\left(\frac{r}{(1-\Omega t)^{1/\gamma}}\right)^{2/(\gamma-1)}\right),$$

and

$$\tilde{u}(r,t) = -\frac{\Omega r}{\gamma(1-\Omega t)}.$$

We choose for the initial density at the origin $\bar{\rho}_0 = 1$, the initial radius is $R_0 = 1$ and the final time of the compression is $T_f = 0.5$. Furthermore, the pressure law is defined by $K = 1$ and $\gamma = 2$. In the simulations, we consider a rectangular domain of size $[0, L_x] \times [0, L_y]$ with $L_x = L_y = 2$ which is discretized with a uniform Cartesian mesh.

Fig. 7–9 present error results as functions of time for different meshes: $\Delta x = \Delta y = 2/50$, $\Delta x = \Delta y = 2/100$ and $\Delta x = \Delta y = 2/200$.

Fig. 7 shows the relative error in L^2 norm between the analytic and the approximate densities. Let us define this norm, we denote by $K = 2/\Delta x = 2/\Delta y$, then the approximate density is a piecewise constant function given by $\rho_{\text{app}}(x,y,t) = \rho_{i,j}^m$ for $x \in [(i-1)\Delta x, i\Delta x)$, $y \in [(j-1)\Delta y, j\Delta y)$ and $t \in [t^m, t^{m+1})$ with $i,j \in \{1,\ldots,K\}$ and $(t^m)_{m\geqslant 0}$ the sequence of the discrete times. We project the exact solution on this space of piecewise constant functions, defining $\rho_{\text{ex}}(x,y,t) = (\rho_{\text{ex}})_{i,j}^m$ for $x \in [(i-1)\Delta x, i\Delta x)$, $y \in [(j-1)\Delta y, j\Delta y)$ and $t \in [t^m, t^{m+1})$ with $i,j \in \{1,\ldots,K\}$ and $m \geqslant 0$. For defining $(\rho_{\text{ex}})_{i,j}^m$, we first introduce $C_{k,i,j} = (x_{k,i,j}, y_{k,i,j})$, for $k = 1,\ldots,4$, the vertices of the square $[(i-1)\Delta x, i\Delta x] \times [(j-1)\Delta y, j\Delta y]$. We denote by $\mathscr{C}_{i,j}^{\text{int},m} = \{k \in \{1,\ldots,4\};$

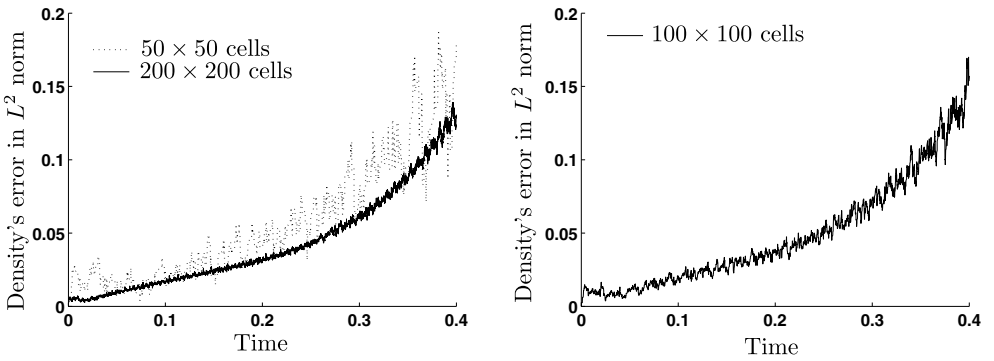

Fig. 7. L^2 relative error on the fluid density as a function of time for different meshes: $\Delta x = \Delta y = 2/50$ and $\Delta x = \Delta y = 2/200$ (left), $\Delta x = \Delta y = 2/100$ (right). The "100×100 cells" curve is between the "200×200 cells" and "50×50 cells" curves.

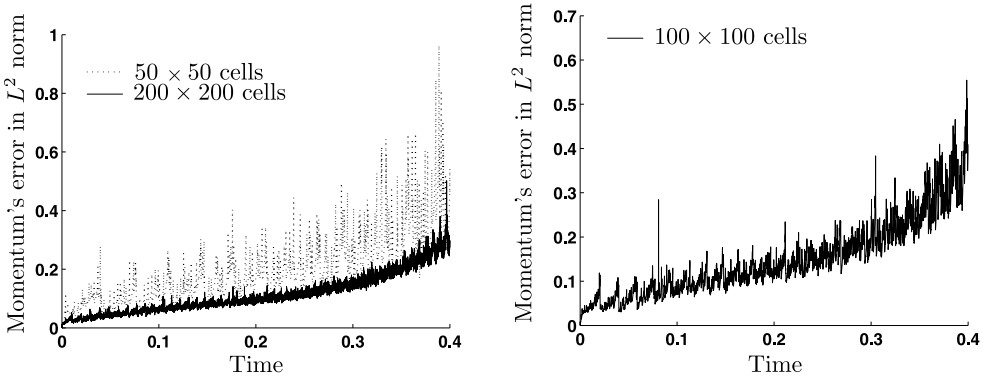

Fig. 8. L^2 relative error on the fluid momentum as a function of time for different meshes: $\Delta x = \Delta y = 2/50$ and $\Delta x = \Delta y = 2/200$ (left) and $\Delta x = \Delta y = 2/100$ (right). The "100×100 cells" curve is between the "200×200 cells" and "50×50 cells" curves.

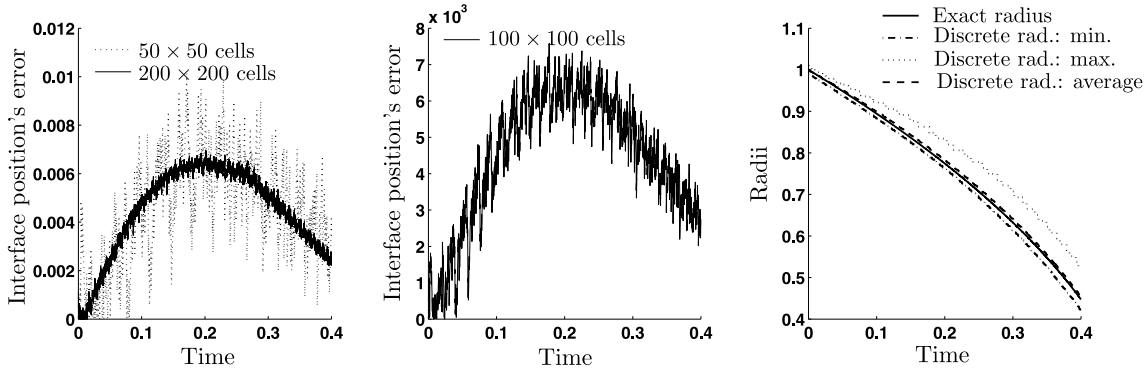

Fig. 9. Left and middle: Relative error on the fluid–vacuum interface position, for $\Delta x = \Delta y = 2/50$ and $\Delta x = \Delta y = 2/200$ (left) and $\Delta x = \Delta y = 2/100$ (middle). The approximate values of the fluid–vacuum interface positions are given by the averaged value of the distance between the origin and the center of all border cells (see Fig. 3 for the definition of border cells). The "100×100 cells" curve is between the "200×200 cells" and "50×50 cells" curves. Right: exact and approximate values of the plasma–vacuum interface position as functions of time for $\Delta x = \Delta y = 2/100$. The approximate values are the minimum, the maximum and the averaged value of the distance between the origin and the center of all border cells.

$\sqrt{|x_{k,i,j}|^2 + |y_{k,i,j}|^2} \leqslant R(t^m)\}$, then $(\rho_{\text{ex}})^m_{i,j} = \frac{1}{\text{card}(\mathscr{C}^{\text{int},m}_{i,j})} \sum_{l \in \mathscr{C}^{\text{int},m}_{i,j}} \rho(C_{k,i,j}, t^m)$ where ρ is the exact solution defined by (23) and $\text{card}(\mathscr{C}^{\text{int},m}_{i,j})$ is the cardinal of the set $\mathscr{C}^{\text{int},m}_{i,j}$. The relative error between the analytic and the approximate densities in L^2 norm is given by

$$\left(\sum_{i=1}^{K} \sum_{j=1}^{K} \Delta x \Delta y \left| \rho^m_{i,j} - (\rho_{\text{ex}})^m_{i,j} \right|^2 \right)^{1/2} \Bigg/ \left(\sum_{i=1}^{K} \sum_{j=1}^{K} \Delta x \Delta y \left| (\rho_{\text{ex}})^m_{i,j} \right|^2 \right)^{1/2}. \tag{24}$$

Fig. 8 gives the relative error between the analytic and the approximate momentums. We can see that the numerical solution converges to the analytic solution since the errors on the density and and on the momentum are decreasing while the mesh is refined. The left and middle pictures of Fig. 9 give the relative error between the exact and approximate radii of the fluid bubble. The exact radius is given by (22) and the approximate radius is obtained with an averaged value of the distance between the origin and the center of all border cells (see Fig. 3 for the definition of border cells). The right picture of Fig. 9 presents the exact radius and different values for the approximate radius: the previous averaged value, the minimum and maximum values of the distance between the origin and the center of all border cells. We can see that even if the error between the exact radius and the averaged value is decreasing from time $t = 0.2$ the approximation of the radius

is less and less accurate since the variance increases. But, even with a rough mesh (50×50 cells) the error on the interface position is of order 1.% and so it is very small. This is an important property for our problem since we recall that getting precisely the interface position is a key point in the high current diodes problem because it governs the value of the current in the electron beam. Figs. 10–12 give an L^∞ comparison between the exact and the approximate densities at times $t = 0.07$ and $t = 0.3$. We can see that the error is large on border cells but small on interior cells. This error increases with time but does not introduce instabilities since in the interior cells the error is still small at time $t = 0.3$. Fig. 13 shows the same behavior of the scheme on the momentum. Right pictures of Figs. 11, 12 and the bottom right picture of Fig. 13 present the error on the density and momentum for interior cells. We can see that the scheme has a good agreement with the exact solution in the interior of the fluid bubble. Fig. 14 presents the fluid bubble for different times, on the top given by the approximate solution with $\Delta x = \Delta y = 2/50$, in the middle given by the approximate solution with $\Delta x = \Delta y = 2/200$ and on the bottom given by the exact solution. We can see that the approximate bubble becomes square while the exact bubble is circular. This is due to the numerical algorithm and more precisely to the splitting of the Euler system into systems (14) and to the SLIC algorithm used in the projection step. Indeed with systems (14) the transport in the directions x and y are decoupled and this privileges the Cartesian deformations. Furthermore, the SLIC algorithm gives a square reconstruction of the interface and increases this phenomena. Fig. 14 shows that the convergence towards a circular bubble is very slow since multiplying the number of cells by 4×4, the difference between the results is not significant. This point will have to be ameliorated in future works. This can be done discretizing directly system (4) instead of systems (14) and using Youngs' method (see [60]) instead of the SLIC algorithm in the projection step. This error on the location of border cells explains the important errors encountered on the density and momentum for border cells, see left pictures of Figs. 11, 12 and the bottom left picture of Fig. 13. It is important to note that in spite of the bad approximation of the density and velocity for border cells, we have a very good prediction of the mean interface position (see Fig. 9, right). Furthermore, we stress that Fig. 14 shows that we have the right behavior of the bubble and the *right compression time* since at exactly $t = 0.5$ the numerical bubble has disappeared completely of the domain like the exact bubble.

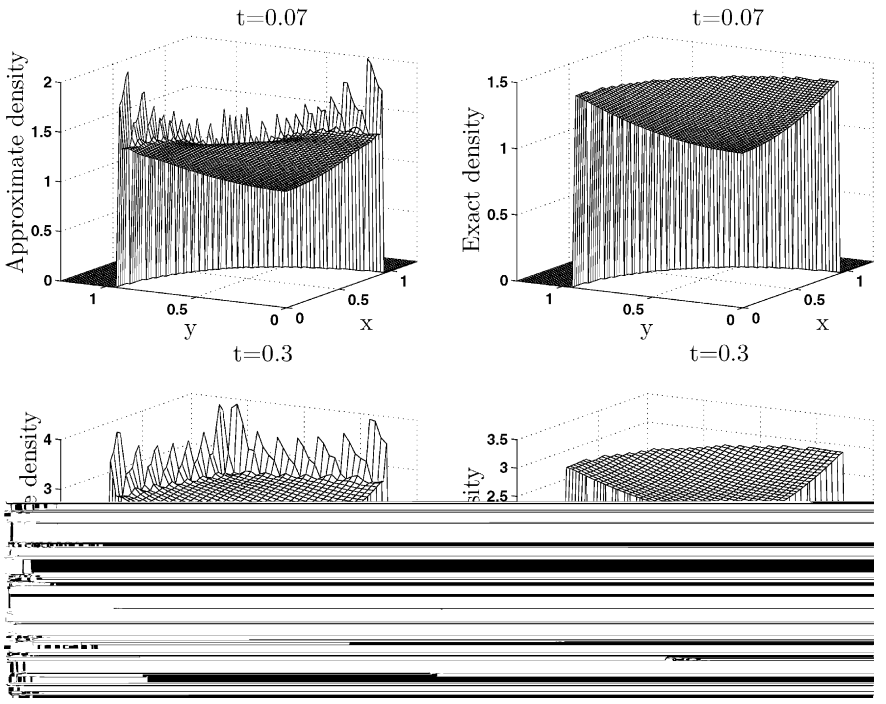

Fig. 10. On the left: approximate density given by the VOF scheme presented in Section 3 at times $t = 0.07$ and $t = 0.3$ for $\Delta x = \Delta y = 2/100$. On the right: exact density given by (23) at times $t = 0.07$ and $t = 0.3$. It is projected on the mesh.

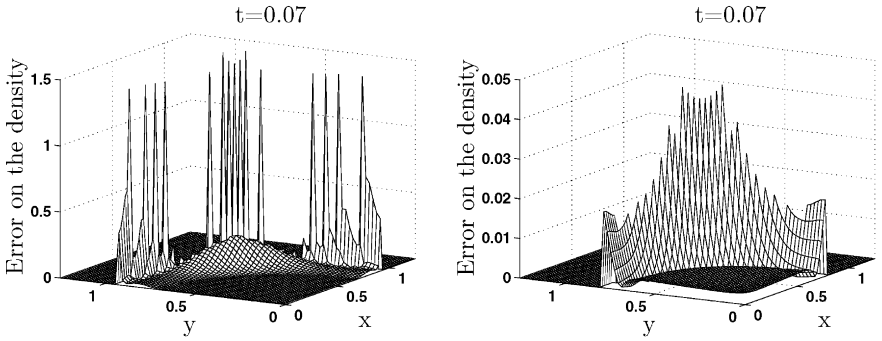

Fig. 11. Difference between the exact and the approximate densities at time $t = 0.07$, on the left for all the fluid bubble and on the right only for interior cells. The approximate density is given by the VOF scheme presented in Section 3 for $\Delta x = \Delta y = 2/100$. The exact density is given by (23) and is projected on the mesh.

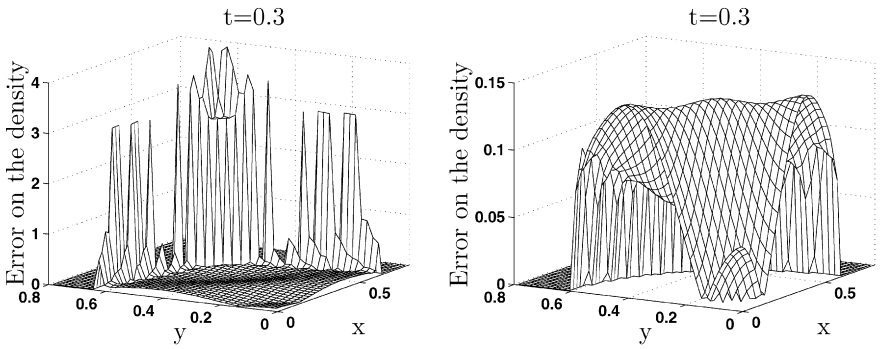

Fig. 12. Difference between the exact and the approximate densities at time $t = 0.3$, on the left for all the fluid bubble and on the right only for interior cells. The approximate density is given by the VOF scheme presented in Section 3 for $\Delta x = \Delta y = 2/100$. The exact density is given by (23) and is projected on the mesh.

4.2. High current diodes

The accuracy of the scheme, detailed in Section 3, has been studied when an homogeneous pressure is applied on the surface of a fluid bubble. Now, we present results for high current diodes. We recall that the asymptotic model of Section 2 has been proposed to describe such a device. We approximate it with the VOF method presented in Section 3. Physical parameters for high current diodes (see [30,34,48,55,58] for a more precise description of high current diodes) are chosen such that the distance between electrodes $L = 10^{-2}$ m, the heat specific ratios: $\gamma_i = \gamma_e = 5/3$ and $C_i = C_e = 1$. We consider protons and electrons, then $m_i = 3.37 \times 10^{-27}$ kg and $m_e = 9.1 \times 10^{-31}$ kg. The temperature, the density and the velocity at the injection point are chosen such that: $T_i = T_e = 5$ eV, $n_i = n_e = n_0 = 10^{20}$ m^{-3} and $u_i = u_e = u_0 = \sqrt{eT_i/m_i} = 1.5 \times 10^4$ m/s, where we recall that $e = 1.6 \times 10^{-19}$ C is the positive elementary charge. Finally, the applied potential is defined by $\phi(x = 0) = 0$ V and $\phi(x = L) = \phi_L = 10^5$ V.

In the following simulations, we consider a square domain and the injection region for the plasma is assumed to be small, of size $2\Delta x$ such that the artificial boundary Γ_{art} does not act on the plasma expansion. We discretize the domain with a uniform Cartesian mesh constituted of 100×100 cells. Moreover, the one-dimensional study of such a device (see [12]) shows that in order to get the right interface position, the reaction-pressure acting along the interface must be penalized by the coefficient $\alpha = 0.5$.

Fig. 15 presents the density in the region filled by the plasma for time $t = 0.10\tau$, $t = 0.20\tau$, $t = 0.30\tau$ and $t = 0.40\tau$. The plasma bubble expands from the cathode to the anode. It is slowed down by the reaction pressure force which expresses the reaction of the plasma to the emission of electrons in the beam. We recall that we have chosen a free current model with a reaction pressure force located at the plasma–beam interface only.

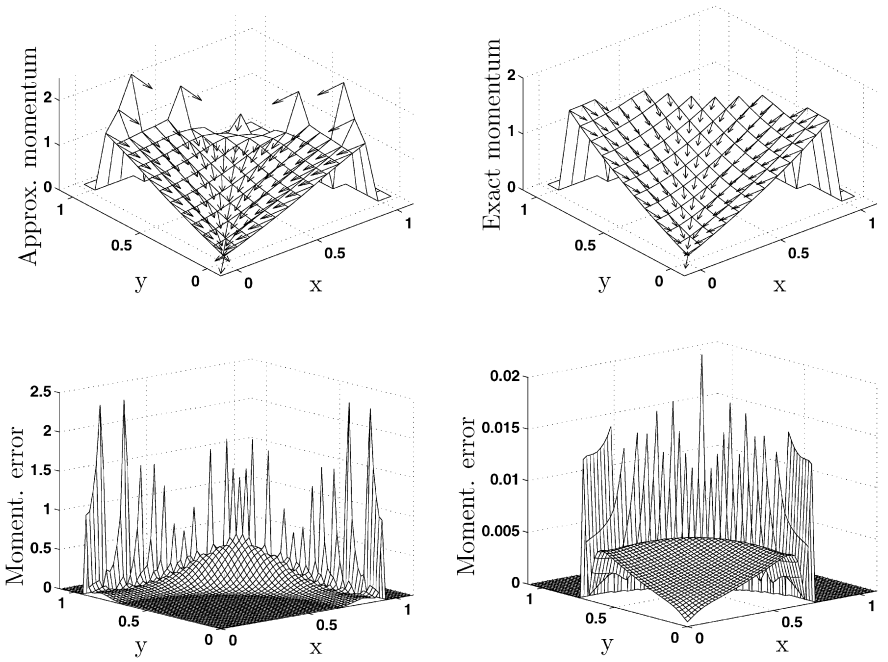

Fig. 13. Top: Euclidean norms of the approximate momentum (left) and of the exact momentum (right) at time $t = 0.07$. Bottom: Difference between the Euclidean norms of the exact and approximate momentums at time $t = 0.07$, on the left for all the fluid bubble, on the right only for interior cells. The approximate momentum is given by the VOF scheme presented in Section 3 for $\Delta x = \Delta y = 2/100$. The exact momentum is given by (23) and is projected on the mesh.

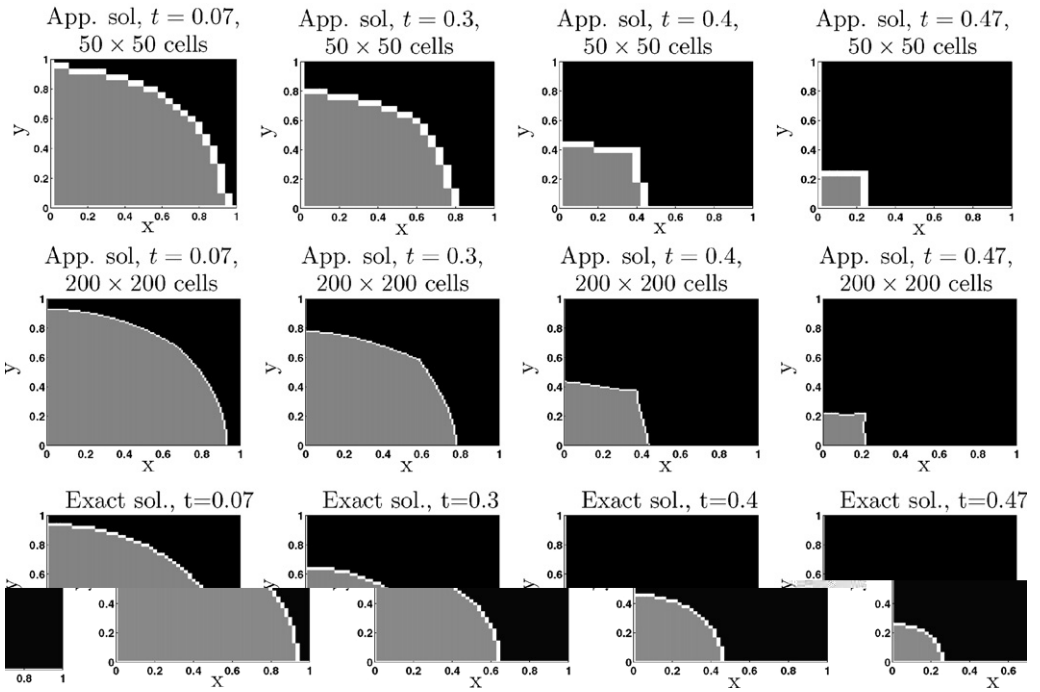

Fig. 14. Fluid bubble for different times $t = 0.07$, $t = 0.3$, $t = 0.4$ and $t = 0.47$. We can see the different type of the cells: in gray, the full cells, in white, the mixed cells and in black, the empty cells. Top and middle, the results are computed with the VOF scheme presented in Section 3 with $\Delta x = \Delta y = 2/50$ (top) and $\Delta x = \Delta y = 2/200$ (middle). Bottom: the results are computed with the exact solution given by (23) and projected on the mesh.

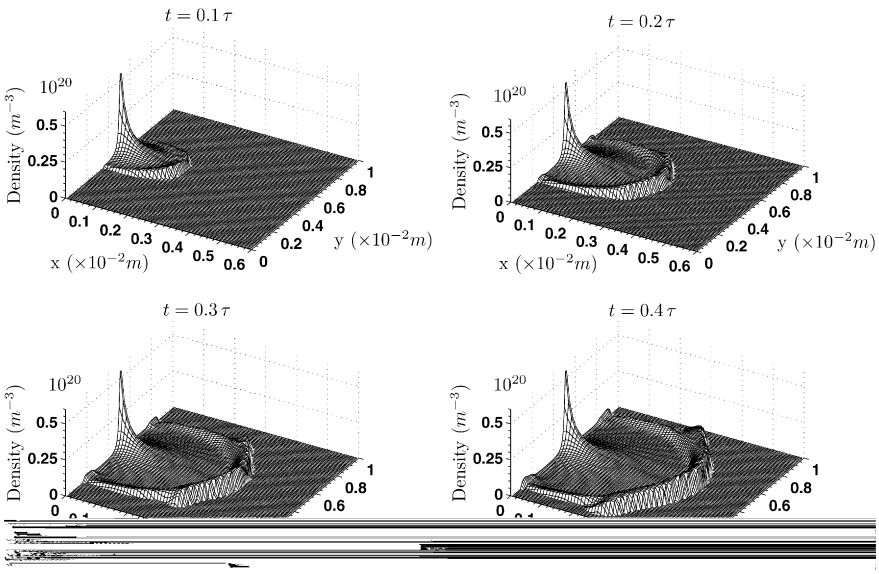

Fig. 15. Plasma density at the time $t = 0.1\tau$, $t = 0.2\tau$, $t = 0.3\tau$, $t = 0.4\tau$ with $\tau = u_0/L = 6.67 \times 10^{-7}$ s. The solution is computed with the discretized asymptotic model using the VOF scheme presented in Section 3. We use a uniform Cartesian mesh with 100×100 cells.

We can observe that due to this reaction-pressure force, the plasma region keeps connected during the simulation, there is no instabilities at the interface. Hence, Fig. 16 presents the projections of the density in the x direction. It shows more precisely the effect of the reaction-pressure term: the front of the plasma is very stiff

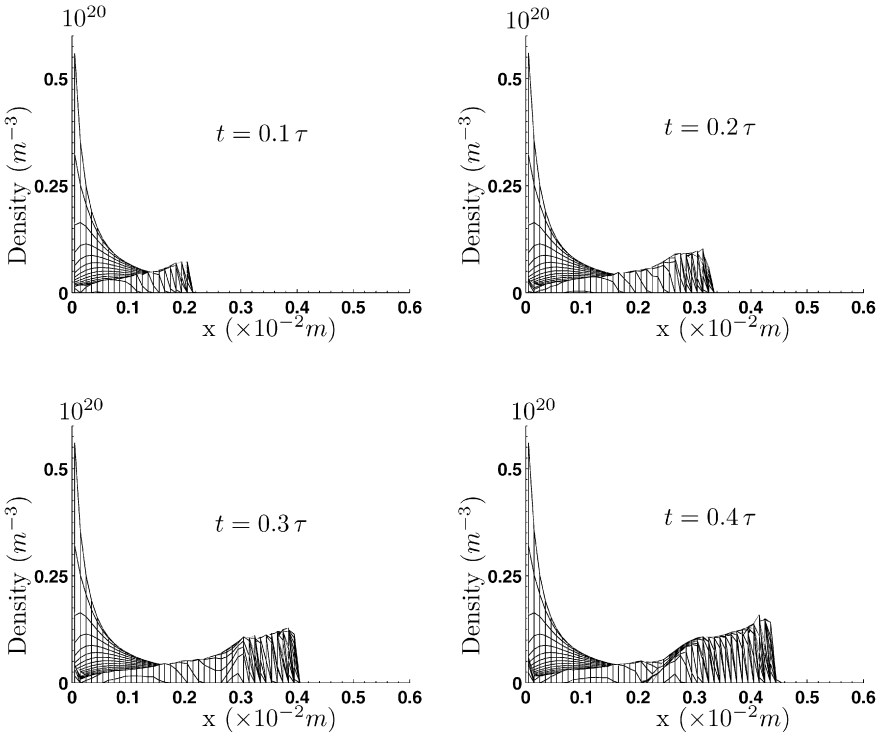

Fig. 16. Orthogonal projection on $[0, x)$ of the plasma density at the time $t = 0.1\tau$, $t = 0.2\tau$, $t = 0.3\tau$, $t = 0.4\tau$ with $\tau = u_0/L = 6.67 \times 10^{-7}$ s. The solution is computed with the discretized asymptotic model using the VOF scheme presented in Section 3. We use a uniform Cartesian mesh with 100×100 cells.

near the interface. Note that, like in one-dimensional simulations, see [12,14], we observe a non-physical overflow in the density results at the plasma–beam interface. This is due to the model and more precisely to the fact that the reaction-pressure force should be exerted in all the plasma and not only at the plasma–beam interface. We recall that in one dimension in spite of this, the interface position is well predicted. A possible way to overcome this problem consists in using a quasi-neutral model with a non vanishing current for the description of the plasma, see [13] for one-dimensional numerical results. In Fig. 15, we can also note that the physical symmetry of the plasma bubble with rapport to the line $y = 0.5$ is well described by the numerical solution. Indeed, let us denote by n_{app} the piecewise constant approximation of the density n. This approximation is defined by $n_{\text{app}}(x, y, t) = n^m_{i,j}$ for all $x \in [(i-1)\Delta x, i\Delta x)$, $y \in [(j-1)\Delta y, j\Delta y)$ and $t \in [t^m, t^{m+1})$ with $i, j \in \{1, \ldots, 100\}$ and $(t^m)_{m \geqslant 0}$ the sequence of the discrete times. We define the L^1 error on the symmetry by $err(t) = \sum_{i=1}^{100}\sum_{j=1}^{50} \Delta x\Delta y|n^m_{i,j} - n^m_{i,100-j+1}| / \sum_{i=1}^{100}\sum_{j=1}^{50}\Delta x\Delta y|n^m_{i,j}|$ if $t \in [t^m, t^{m+1})$. Then, the error on the symmetry for the different times plotted in Fig. 15 are given by $err(0.1\tau) \approx 1.2 \times 10^{-13}$, $err(0.2\tau) \approx 9.4 \times 10^{-13}$, $err(0.3\tau) \approx 1.05 \times 10^{-12}$ and $err(0.4\tau) \approx 1.74 \times 10^{-9}$. This shows that the symmetry is well described by the approximate solution. Fig. 17 shows the plasma velocity. The effect of the reaction-pressure term is confirmed here since the L^2 norm of the velocity vector is smaller near the interface than in the plasma bubble. This difference increases with time, this is due to the fact that the pressure reaction force increases when the distance between the interface and the anode decreases. Furthermore, Fig. 17 shows an azimuthal asymmetry. At times $t = 0.1\tau$ and $t = 0.2\tau$ the plasma bubble is oval. This shape is physical. Indeed, the electrons are accelerated in the x-direction because of the positive potential of the anode located on the plane $x = 1$. Then, the ions try to follow the electrons for quasi-neutrality reasons, and the plasma bubble becomes oval. At times $t = 0.3\tau$ and $t = 0.4\tau$ there is a deformation on the front of the bubble. This shape is no more physical. Like for the non-physical overflow in the density results at the plasma–beam interface, this deformation is due to the model and more precisely to the reaction-pressure force. Indeed, this force should be exerted in all the plasma. But in our model, it is located at the plasma–beam interface. Then, the reaction-pressure force is too large at the

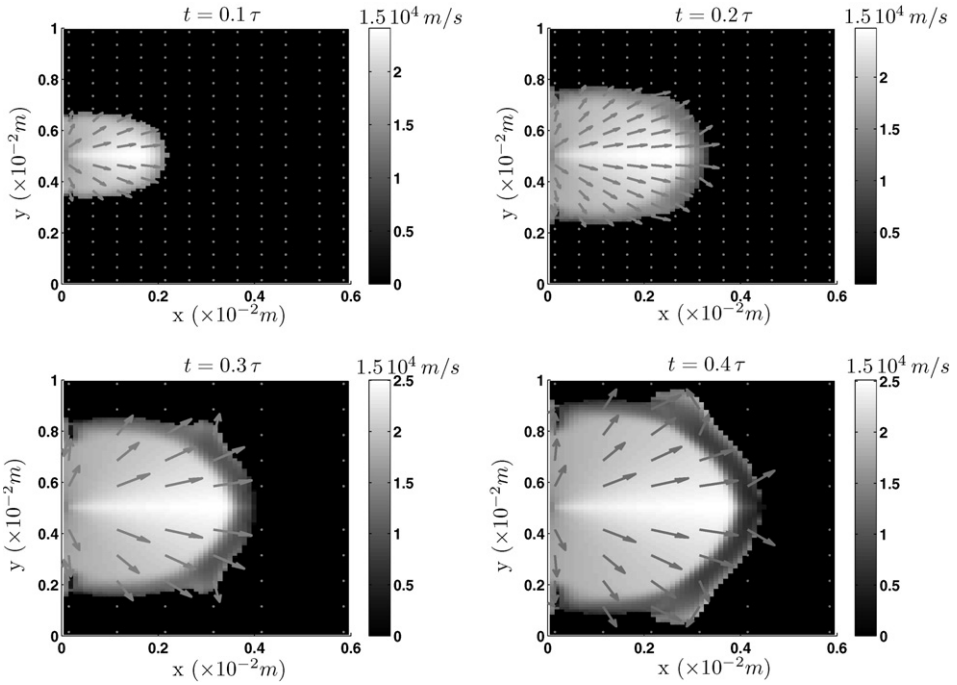

Fig. 17. Plasma velocity at the time $t = 0.1\tau$, $t = 0.2\tau$, $t = 0.3\tau$, $t = 0.4\tau$ with $\tau = u_0/L = 6.67 \times 10^{-7}$ s. The solution is computed with the discretized asymptotic model using the VOF scheme presented in Section 3. We use a uniform Cartesian mesh with 100×100 cells. The vectors indicate the direction of the velocity vector and the color gives the L^2 norm of the velocity vector.

plasma–beam interface and leads to unphysical deformations of the plasma bubble. We recall that the quasi-neutral plasma model with a non-vanishing current proposed in [13] gives a model for which the pressure-reaction force is exerted continuously in all the plasma region. Then, using this model would certainly allow to overcome this problem.

5. Conclusion

In this paper, we proposed a simplified two-dimensional model for the description of a plasma bubble expansion between two electrodes. This model is an extension of the one-dimensional model of [12] obtained by a formal asymptotic analysis, from the two-fluid Euler–Poisson model. This model is constituted of the isentropic Euler equations for the quasi-neutral fluid. For the beam region we proposed a simplified Child–Langmuir model. It consists in assuming that the one-dimensional Child–Langmuir law can be applied. For all points of the plasma–beam interface, knowing the distance covered by an electron from this point to the anode, the one-dimensional Child–Langmuir law gives the current at the plasma–beam interface point. We proposed a simple method to approximate this covered distance.

Furthermore, we described the numerical scheme used for the discretization of this model. This is a volume of fluid method with the SLIC algorithm (simple line interface calculation). We detailed the numerical processing of the ''pressure reaction'' term acting along the discrete interface. We gave numerical results for a test case of a two-dimensional fluid compression for which we can compare the numerical solution to an analytical solution. Then we performed numerical simulations of the high current diodes problem.

These preliminary results of the numerical plasma–beam interface tracking give promising results which can be extended to more complex models. Indeed with the two-dimensional fluid compression test case we have seen that we have the right compression time and a good approximation, with the mean value, of the bubble radius. The splitting of the system into the transport in the directions x and y and the SLIC algorithm privilege the Cartesian deformations, and at the end of the simulation the approximate bubble becomes square while the exact bubble is circular. This point can be ameliorated discretizing directly system (4) instead of the splitted systems (14) and using Youngs' method (see [60]) instead of the SLIC algorithm in the projection step.

In the case of the high current diodes problem, the plasma bubble expansion is well described. A generalization of this work to a non-zero current model, like the one proposed in [13] for the one-dimensional case, would be interested in order to better approximate the plasma density, i.e., without the overflow at the plasma–beam interface. Then, a comparison with the results obtained in [11] using an asymptotic preserving scheme would offer attractive perspectives.

References

[1] D.J. Benson, Computational methods in Lagrangian and Eulerian hydrocodes, Comput. Methods Appl. Mech. Eng. 99 (1992) 235.
[2] S. Bouquet, Une solution analytique décrivant la compression d'un milieu soumis à une pression extérieure uniforme, CEA private communication.
[3] J. Brackbill, D.B. Kothe, C. Zemach, A continuum method for modeling surface tension, J. Comput. Phys. 100 (1992) 335.
[4] Y.C. Chang, T.Y. Hou, B. Merriman, S. Osher, A level set formulation of Eulerian interface capturing methods for incompressible fluid flows, J. Comput. Phys. 124 (1996) 449.
[5] F.F. Chen, Introduction to Plasma Physics, Plenum, New York, 1974.
[6] M. Cho, Arcing on high voltage solar arrays in low earth orbit: theory and computer particle simulation, Ph.D. Thesis, Massachusetts Institute of Technology, 1992.
[7] H.-H. Choe, N.S. Yoon, S.S. Kim, D.-I. Choi, A new unconditionally stable algorithm for steady-state fluid simulation of high density plasma discharge, J. Comput. Phys. 170 (2001) 550–561.
[8] A.J. Chorin, Flame advection and propagation algorithms, J. Comput. 35 (1980) 1.
[9] P. Colella, M.R. Dorr, D.D. Wake, A conservative finite difference method for the numerical solution of plasma fluid equations, J. Comput. Phys. 149 (1999) 168–193.
[10] P. Crispel, P. Degond, M.H. Vignal, Quasi-neutral fluid models for current carrying plasmas, J. Comput. Phys. 205 (2005) 408.
[11] P. Crispel, P. Degond, M.-H. Vignal, An asymptotic preserving scheme for the two-fluid Euler-Poisson model in the quasi-neutral limit, J. Comput. Phys. 223 (2007) 208–234.
[12] P. Degond, C. Parzani, M.H. Vignal, Un modéle d'expansion de plasma dans le vide, C. R. Acad. Sci. Paris 335 (2002) 399.
[13] P. Degond, C. Parzani, M.H. Vignal, Plasma expansion in vacuum: modeling the breakdown of quasineutrality, SIAM, Multiscale Model. Simul. 2 (2003) 158.

[14] P. Degond, C. Parzani, M.H. Vignal, A model for plasma expansion in the vacuum, in: Proceedings of the conference "Free Boundary Problems 2002, Trento, June 2002.
[15] P. Degond, P.F. Peyrard, G. Russo, Ph. Villedieu, Polynomial upwind schemes for hyperbolic systems, C. R. Acad. Sci. Paris, Ser. I 328 (1999) 479.
[16] P. Degond, P.A. Raviart, An asymptotic analysis of the one-dimensional Vlasov–Poisson system: the Child–Langmuir law, Asymptot. Anal. 4 (1991) 187.
[17] P. Degond, P.A. Raviart, On a penalization of the Child–Langmuir emission condition for the one-dimensional Vlasov–Poisson equation, Asymptot. Anal. 6 (1992) 1.
[18] P. Degond, R. Talaalout, M.H. Vignal, Electron transport and secondary emission in a surface of solar cell, in: Proceeding of the Workshop 'Multipactor, RF and DC Corona and Passive Intermodulation in Space RF Hardware', ESTEC, Noordwijk, The Netherlands, 4–6 September, 2000.
[19] Sylvie Fabre, Stability analysis of the Euler–Poisson equations, J. Comput. Phys. 101 (1992) 445.
[20] M. Friedman, V. Serlin, A. Drobot, L. Seftoz, Self modulation of an intense relativistic electron beam, J. Appl. Phys. 56 (1984) 2459.
[21] J. Glimm, O. Mc Bryan, D.H. Sharp, Front tracking applied to Rayleigh–Taylor instability, SIAM J. Sci. Stat. Comput. 7 (1986) 230.
[22] J. Glimm, J.W. Grove, X.L. Li, D.C. Tan, Robust computational algorithms for dynamic interface tracking in three dimensions, SIAM J. Sci. Comput. 6 (21) (2000) 2240.
[23] S.Y. Ha, M. Slemrod, Global existence of plasma ion sheaths and their dynamics, Comm. Math. Phys. 238 (2003) 149.
[24] D.E. Hastings, M. Cho, H. Kuninaka, Arcing rates for high voltage solar arrays: theory, experiments and predictions, J. Spacecraft Rockets 29 (1992) 538.
[25] C.W. Hirt, J.L. Cook, T.D. Butler, A Lagrangian method for calculating the dynamics of an incompressible fluid with free surface, J. Comput. Phys. 5 (1970) 103.
[26] C.W. Hirt, B.D. Nichols, Volume Of Fluid (VOF) method for the dynamics of free boundaries, J. Comput. Phys. 39 (1982) 201.
[27] S. Karni, Multicomponent flow calculations by a consistent primitive algorithm, J. Comput. Phys. 112 (1994) 31.
[28] I. Katz, D.B. Snyder, E.A. Robertson, ESD triggered solar array failure mechanism, in: 6th Spacecraft Charging Technology Conference, AFRL-VS-TR-20001578, September, 2000.
[29] N.A. Krall, A.W. Trivelpiece, Principles of Plasma Physics, San Francisco Press, 1986.
[30] Ya.E. Krasik, A. Dunaevsky, A. Krokhmal, J. Felsteiner, Emission properties of different cathodes at $E \leqslant 10^5$ V/cm, J. Appl. Phys. 89 (4) (2001) 2379.
[31] I. Langmuir, K.T. Compton, Electrical discharges in gases, part II, fundamental phenomena in electrical discharges, Rev. Mod. Phys. 3 (1931) 191.
[32] R.J. LeVeque, Finite volume methods for hyperbolic problems, Cambridge Texts in Applied Mathematics, Cambridge University Press, Cambridge, 2002.
[33] J. Maenchen, G. Cooperstein, J. O'Malley, I. Smith, Advances in pulsed power-driven radiography systems, Proc. IEEE 92 (7) (2004) 1021.
[34] R.B. Miller, Mechanism of explosive electron emission for dielectric fiber (velvet) cathodes, J. Appl. Phys. 84 (7) (1998) 3880.
[35] J.P. Morris, Simulating surface tension with smoothed particle hydrodynamics, Int. J. Numer. Meth. Fluids 33 (2000) 333.
[36] W.F. Noh, P. Woodward, SLIC – Simple Line Interface Calculation, in: A.I. van Dooren, P.J. ZAndbergen (Eds.), Lecture Notes in Physics, vol. 59, Springer, New York, 1976, p. 330.
[37] S. Osher, R. Fedkiw, Level Set Methods and Dynamic Implicit Surfaces, Springer, New York, 2003.
[38] S. Osher, J.A. Sethian, Fronts propagating with curvature dependent speed: algorithms based on Hamilton–Jacobi formulations, J. Comput. Phys. 79 (1988) 12.
[39] C. Parzani, Modélisation Mathématique d'Expansion de Plasma et de Décharges Electriques, Ph.D. Thesis, INSA Toulouse, December, 2003.
[40] S. Popinet, S. Zaleski, A front-tracking algorithme for accurate representation of surface tension, Int. J. Numer. Meth. Fluids 30 (1999) 775.
[41] K.U. Riemann, The Bohm criterion and sheath formation, J. Phys. D 24 (1991) 493.
[42] M. Rudman, Volume-tracking methods for interfacial flow calculations, Int. J. Numer. Meth. Fluids 24 (1997) 671.
[43] R. Saurel, R. Abgrall, A simple method for compressible multifluid flows, SIAM J. Sci. Comput. 21 (3) (1999) 1115.
[44] R. Scardovelli, S. Zaleski, Interface reconstruction with least-square fit and split Eulerian–Lagrangian advection, Int. J. Numer. Meth. Fluids 41 (2003) 251.
[45] R. Schneider, C.-D. Munz, The approximation of two-fluid plasma flow with explicit upwind schemes, Int. J. Numer. Model. 8 (2005) 399–416.
[46] D. Serre, Systems of Conservation Laws, vol. 1, Cambridge University Press, Cambridge, 1999.
[47] J.A. Sethian, Level Set Methods and Fast Marching Methods: Evolving Interfaces in Computational Geometry, Fluid Mechanics, Computer Vision, and Materials Science, Cambridge University Press, Cambridge, 1999.
[48] D. Shiffer, M. Ruebush, D. Zagar, M. LaCour, M. Sena, K. Golby, M. Haworth, R. Umstattd, Cathode and anode plasma in short-pulse explosive field emission cathodes, J. Appl. Phys. 91 (9) (2002) 5599.
[49] U. Shumlak, J. Loverich, Approximate Riemann solver for the two-fluid plasma model, J. Comput. Phys. 187 (2003) 620–638.
[50] M. Slemrod, Shadowing and the plasma–sheath transition layer, J. Nonlinear Sci. 11 (193) (2001).
[51] M. Slemrod, The radio frequency driven plasma sheath: asymptotics and analysis, SIAM J. Appl. Math. 63 (1737) (2003).
[52] A. Smolianski, Finite-element/level-set/operator-splitting (FELSOS) approach for computing two fluid unsteady flows with free moving interfaces, Int. J. Numer. Meth. Fluids 48 (2005) 231.

[53] M. Sussman, A.S. Almgren, J.B. Bell, P. Colella, L.H. Howell, M.L. Welcome, An adaptive level set approach for incompressible two-phase flows, J. Comput. Phys. 148 (1999) 81.
[54] M. Sussman, P. Smereka, S. Osher, A level set approach for computing solutions to incompressible two-phase flow, J. Comput. Phys. 114 (1994) 146.
[55] H. Sze, J. Benford, W. Woo, B. Harteneck, Dynamics of a virtual cathode oscillator driven by a pinched diode, Phys. Fluids 29 (1986) 3873.
[56] S.O. Unverdi, G. Tryggvason, A front-tracking method for viscous, incompressible, multi-fluid flows, J. Comput. Phys. 100 (1992) 25.
[57] T. Weisterman, A particle-in-cell method as a tool for diode simulations, Nucl. Instr. Methods Phys. Res. A 263 (1988) 271.
[58] M. Yatsuzuka, M. Nakayama, M. Tanigawa, S. Nobuhara, D. Young, O. Ishihara, Plasma effects on electron beam focusing and microwave emission in a virtual cathode oscillator, IEEE Trans. Plasma Sci. 26 (4) (1998) 1314.
[59] D.L. Youngs, Time dependent multi-material flow with large fluid distortion, in: K.W. Morton, M.J. Baines (Eds.), Numerical Methods for Fluid Dynamics, Academic Press, London, New York, 1982, p. 273.
[60] D.L. Youngs, An interface tracking method for a 3D Eulerian hydrodynamics code, Report of Atomic Weapons Research Establishment, 1994.